Max-Planck-Institut für Quantenoptik

Technische Universität München

Remote Entanglement of Two Single Atoms

Carolin Hahn

Für meine Eltern

und meinen lieben Freund Chandra.

Abstract

This thesis reports on the generation of entanglement between two single atoms, located in different laboratories at a distance of 21 m. The entanglement is established in the conceptually most fundamental way—by the exchange of a single photon. High-fidelity entanglement between one of the atoms and a single photon is efficiently generated by employing a high-finesse optical resonator that strongly enhances the coupling between light and matter. This enhanced coupling also facilitates the faithful mapping of the quantum state of the photon onto the spin state of the second atom, thereby converting the atom-photon entanglement into remote entanglement between the two atoms. The high success probability and fidelity, and the long coherence times we achieve demonstrate that systems based on single-emitter quantum memories in cavities are promising candidates to form the building blocks of future quantum repeater architectures, representing a realistic avenue towards quantum communication over arbitrary distances.

Zusammenfassung

Die vorliegende Arbeit berichtet über die Verschränkung zweier Einzelatome, die sich im Abstand von 21 m in verschiedenen Laboratorien befinden. Erzeugt wird die Verschränkung auf die konzeptionell einfachste Art und Weise – durch den Austausch eines einzelnen Photons. Der Einsatz eines optischen Resonators mit hoher Finesse ermöglicht die effiziente Erzeugung von Verschränkung zwischen einem der Atome und einem Photon mit hoher Fidelity. Die durch den Resonator verstärkte Licht-Materie-Wechselwirkung ermöglicht auch das Abspeichern des photonischen Polarisationszustandes im anderen Atom. So wird die Atom-Photon-Verschränkung in einen verschränkten Zustand zweier weit von einander entfernter Atome verwandelt. Die hohe Erfolgswahrscheinlichkeit und Fidelity des Verschränkungsprozesses sowie die langen Kohärenzzeiten zeigen, dass Systeme, die auf Einzelemitter-Quantenspeichern in Resonatoren basieren, vielversprechende Kandidanten für die Realisierung zukünftiger Quantenrepeater-Architekturen darstellen, die Quantenkommunikation über beliebig große Distanzen ermöglichen.

Contents

1. Introduction

Until today, entanglement has remained one of the most striking and counterintuitive features of quantum mechanics. For Erwin Schrödinger, who coined the term 'entanglement' in 1935, the phenomenon was not "*one* but rather *the* characteristic trait of quantum mechanics, the one that enforces its entire departure from classical lines of thought" [1]. Entanglement is a consequence of the superposition principle applied to composite systems of two or more particles. In an entangled state, each particle loses its individual quantum identity, and all information about possible measurement outcomes is contained in a global wave function which cannot be decomposed into separate single-particle states.

Measuring the state of one particle of an entangled pair will cause the irreversible collapse of the wave function, thereby instantaneously projecting the quantum state of the other particle of the pair—no matter how far it is away. This non-local character of quantum mechanics, famously described by Einstein as "spooky action at a distance" [2], led Einstein, Podolsky and Rosen to question quantum mechanics. In a seminal paper [3], they argued that quantum mechanics is incomplete if it is assumed that no physical influence can travel faster than the speed of light and that the properties of physical systems are elements of reality.

Almost thirty years later, in the 1960s, John Bell and others proposed experimentally testable conditions using entangled pairs of particles to shed light onto these questions [4, 5, 6, 7]. Bell showed that no local realistic theory can reproduce all predictions made by quantum mechanics, and further that the difference between these predictions is actually measurable. His famous inequality proved that there exists an upper limit to the strengths of observed correlations predicted by local realistic theories – a limit that is violated by the predictions of quantum theory. The proposed tests of Bell's inequality moved the debates and controversies from the realm of theoretical physics out onto the experimental stage.

Not long after, the first experiments showing violations of Bell inequalities followed [8, 9, 10, 11]. In all cases, the experimental results were in convincing agreement with quantum mechanics and posed strong evidence against the existence of local hidden-variable theories, indicating that the description of reality given by the quantum mechanical wave function can indeed be considered complete.

To date, Bell tests have been performed on a variety of systems, including entangled photon pairs [12, 13, 14, 15], low-energy protons [16], neutral kaons [17], ions [18, 19], different degrees of freedom of individual neutrons [20], hybrid systems [21, 22, 23], and single atoms [24]. The final proof for the completeness of quantum mechanics, however, is still outstanding, since all the experiments so far have required additional assumptions depending on their specific construction. This makes them vulnerable to so-called loopholes that leave room for local realistic explanations. A number of experiments have closed either the locality or the detection loophole [13, 15, 18, 25], but the irrefutable loophole-free

Bell test that will finally enforce local realism to be abandoned is yet to be performed. Entangled single atoms at a distance are a strong contender for this measurement [24, 26].

Entanglement is interesting not only from this fundamental point of view. The fascination with the paradoxes of quantum mechanics eventually sparked the development of the new field of quantum information science [27], which promises to radically improve the acquisition, transmission, and processing of information by combining methods from classical information science with fundamental effects of quantum mechanics [28]. Quantum information science has found its way into the mainstream of not only theoretical but also experimental physics, where the possible applications, which may result from the increasing level of control over large scale quantum systems, are currently the focus of enormous research activity. Entanglement is a key resource of many of the applications in this field, such as quantum computation [29] and quantum communication [30, 31, 32].

Controllable quantum systems can be used to construct a quantum computer [33], which has the potential to solve certain problems far more efficiently than any classical computer by making use of quantum superposition and entanglement [34]. Equivalently, well-controlled quantum systems may be used to simulate the physics of other quantum systems in a way that is intractable for classical algorithms, due to the exponential scaling of the Hilbert space with the number of degrees of freedom of the quantum system [35, 36, 37]. Quantum cryptography provides a means for unconditionally secure exchange of information between nodes of a quantum network with ideal source and detection [38]. The security of the encryption is guaranteed by the laws of quantum mechanics, often relying on the properties of entangled particles [30, 39]. Eavesdropping will not go unnoticed, since the no-cloning theorem [40, 41] forbids a potential eavesdropper from simply intercepting the message and resending a copy. However, while the encryption principle itself is absolutely safe, its technical implementation can nevertheless be attacked [42, 43].

Even without the need for encryption, entanglement plays a central role in long distance quantum communication. The bottleneck for communication between remote nodes of a quantum network is the deterioration of the efficiency with the length of the channel connecting the nodes. Optical photons are a natural choice as carriers of quantum information, since a qubit encoded in, for instance, their polarization degree of freedom can be transmitted over long distances with little decoherence. In an optical fiber, however, the probability for both absorption and depolarization of a photon grows exponentially with the length of the fiber. Hence, in a truly large-scale network with distances of hundreds of kilometers between network nodes, simple point-to-point transmission of quantum information becomes infeasible.

A possible solution to this problem is the implementation of a quantum repeater scheme [44]. To this end, one entangles widely separated network nodes, and subsequently uses this entanglement as a resource for quantum teleportation of the qubit to be communicated [31]. In the repeater scheme, quantum memories are located at intermediate locations between the sender and the recipient. In a first step, adjacent memories are entangled pairwise and in parallel using a repeat-until-success scheme. In a second step, entanglement swapping operations are performed between these links to establish entanglement between the sender and the receiver. In a third step, the teleportation step, the sender performs a Bell-state measurement between his part of the entangled pair and the qubit he wants to transmit.

Finally, classical communication of the measurement result enables the recipient to recover the qubit at his site. Using such a repeater scheme has several advantages. The information to be transferred does not have to travel the whole distance via an error-prone channel, but is teleported via a quantum channel generated in a heralded way. Any losses occurring during the build-up of this channel do not affect the fidelity of the information transfer. Most importantly, the time it takes to establish remote entanglement with a quantum repeater scales polynomially with distance [45]. For very large distances, a quantum repeater will therefore outperform any direct entanglement generation attempt, where the time taken to establish entanglement increases exponentially with distance.

Consequently, the capability to efficiently and faithfully generate entanglement between remote quantum memories is an indispensable prerequisite for any future realization of a large-scale quantum network. The work presented in this thesis is at the heart of this application – quantum entanglement is established between two single trapped atoms at nodes of the prototype of an elementary quantum network.

As quantum information is naturally distributed via photons, it is essential that the nodes of a quantum network have an efficient interface with photonic channels. Fully functional network nodes are able to send, receive, and store quantum information reversibly and efficiently. Ideally, they are also capable of creating entanglement between a quantum memory at the node and a single photon. The realization of such quantum nodes poses a major experimental challenge, and different approaches are currently being pursued. Ensembles of gas-phase atoms are an intensely studied example [45, 46, 47], as are solid state systems [48, 49], but the protocols for the generation of single excitations with these systems are inherently probabilistic [50]. Other strong contenders are single particles, such as ions [51], atoms [52, 53, 54], quantum dots [55], color centers in diamond [56], or impurities in silicon [57, 58]. They all allow for single-photon emission [59], quantum gate operations [60, 61, 62], and scalability [63]. Among these possible candidates, single atoms are very promising for future applications since they are among the physical systems with the longest coherence times [64]. However, single emitters generally exhibit only a weak light-matter interaction, again leading to inherently probabilistic information exchange and very low success rates.

A seminal proposal by Cirac and collaborators [65] suggested overcoming these problems by employing network nodes based on single emitters embedded in optical cavities. The cavity-enhanced light-matter interaction opens up a deterministic path for the interconversion of quantum states between light and matter and also – as is of great importance for the experiments presented in this thesis – for the entanglement between quantum states of light and matter. In addition, single particles can be individually addressed, allowing for the realization of deterministic quantum gates [61, 62].

In this thesis, I describe the theoretical and experimental framework for the entanglement of two single atoms at a distance. Unlike all other realizations of remote entanglement of single particles so far [24, 66, 67], which relied on entanglement-swapping, our method of generating remote entanglement is in principle deterministic. It builds on the ability to create entanglement between a single atom and a single photon, and the ability to reversibly exchange a quantum state between a single photon and a single atom.

Chapter 2 focuses on our realization of a single quantum node comprising a single atom

trapped in an optical resonator. I begin with a brief overview of the theoretical background of photon generation and storage, and the theoretical description of entanglement, before introducing the experimental setup. Next, the generation of single photons and atom-photon entanglement is characterized, and the coherent storage and retrieval of a photonic polarization quantum bit with a single-atom quantum memory is discussed. Finally, an account is given of the attempt to collectively enhance the storage efficiency of our quantum memory by working with a small ensemble instead of a single atom in the cavity.

The remote entanglement of two single atoms, located in independent cavity systems in different laboratories at a distance of 21 m, is the topic of chapter 3. We establish the entanglement by creating a photon that is entangled with the atom in laboratory A and then storing this photon in the atom in laboratory B. The results obtained in this experiment are compared with earlier measurements where a single atom was entangled with a Bose-Einstein condensate.

In the concluding chapter 4, I discuss possible improvements of our setup, and the perspectives of atom-cavity systems as a resource in a large-scale quantum information network.

2. An atom-cavity network node for quantum information processing

A fundamental prerequisite for any quantum network is a quantum interconnect that converts flying qubits into stationary qubits and vice versa. As quantum information is naturally distributed via photons, it is essential that the nodes of a quantum network have an efficient interface with photonic channels. Fully functional nodes should be able to send, receive and store photonic quantum information reversibly and efficiently. Ideally, they are also capable of creating entanglement between a quantum memory at the node and a single photon.

This chapter is dedicated to our realization of such a universal network node, comprising a single atom coupled to an optical cavity. The strong interaction between light and matter provided by the cavity facilitates the efficient generation of single photons and of atom-photon entanglement, and enables the mapping between photonic and atomic qubits in a reversible manner. After establishing the fundamental theoretical framework in section 2.1, I turn to the experimental implementation of our atom-cavity quantum node and its characterization. An overview of the experimental setup and all relevant parameters is presented in section 2.2, before the experimental results of the generation of atom-photon entanglement and of the coherent storage of single photons in a single-atom quantum memory are discussed in sections 2.3 and 2.4, respectively. In a detour from experimenting with just a single atom, the storage of weak coherent pulses in an ensemble of atoms in the cavity is explored in Sec. 2.5.

The content of this chapter has partially been published in:
Generation of single photons from an atom-cavity system.
M. Mücke, J. Bochmann, C. Hahn, A. Neuzner, C. Nölleke, A. Reiserer, G. Rempe, and S. Ritter, *Physical Review A* **87**, 063805 (2013)
and
An elementary quantum network of single atoms in optical cavities.
S. Ritter, C. Nölleke, C. Hahn, A. Reiserer, A. Neuzner, M. Uphoff, M. Mücke, E. Figueroa, J. Bochmann, and G. Rempe, *Nature* **484**, 195 (2012)

2.1. Theoretical concepts

The key element of the experiments in this thesis is the reversible conversion between quantum states of light and matter. It is based on the dynamic control of coherent dark states of the atom-cavity system, the theoretical background of which is introduced in section 2.1.1. What entanglement means and how it can be quantified is the topic of section 2.1.2.

2.1.1. Generation and storage of single photons

The mirrors of a cavity set boundary conditions for the electro-magnetic field inside the resonator, resulting in quantized modes. If just one mode is considered, each photon of this mode carries the energy $\hbar\omega_{\text{cav}}$. For an atom placed in this resonator, the coupling strength between the atom and light is described by a coupling constant [68]

$$g(\boldsymbol{r}) = \sqrt{\frac{\omega_{\text{cav}}}{2\hbar\epsilon_0 V}}d_{ge}\psi(\boldsymbol{r}) = g_0 \cdot \psi(\boldsymbol{r}) \tag{2.1}$$

with the cavity mode volume V, vacuum permitivity ϵ_0, the transition dipole matrix element d_{ge} expressing the strength of the atomic transition, and a mode function $\psi(\boldsymbol{r})$ that describes the spatial variation of the electro-magnetic field inside the resonator. In case of the TEM_{00} mode, the spatial modulation of the atom-cavity coupling is given by

$$\psi(\boldsymbol{r}) = \cos\left(\frac{\omega_{\text{cav}}}{c}z\right)\exp\left(-\frac{x^2 + y^2}{w^2}\right), \tag{2.2}$$

where w is the waist of the cavity mode and c the speed of light.

The interaction between the atom and the light field inside the cavity can be used to efficiently create and store single photons, employing a technique called *stimulated Raman adiabatic passage* (STIRAP) [52, 69, 70], the working principle of which will be explained in this section. The interaction between the atom and the light field inside the cavity can be used to efficiently create and store single photons, employing a technique called *stimulated Raman adiabatic passage* (STIRAP) [52, 69, 70], the working principle of which will be explained in this section.

Consider the atom to be a three-level system with two hyperfine ground states $|g\rangle$ and $|u\rangle$ and an excited state $|e\rangle$ coupled in a Λ-configuration, with the two transition frequencies $\omega_{eg} = \omega_e - \omega_g$ and $\omega_{eu} = \omega_e - \omega_u$ (Fig. 2.1). We will initially neglect any kind of dissipation through coupling to the environment. A quantized mode of the cavity is near-resonant with the states $|g\rangle$ and $|e\rangle$ with the frequency ω_{cav} and *vacuum Rabi frequency* $2g$, and an external laser field couples the states $|u\rangle$ and $|e\rangle$ with the frequency ω_c and the *control Rabi frequency* Ω_c. Detunings from the respective atomic transitions are defined as $\Delta_C = \omega_{eu} - \omega_c$ and $\Delta_{\text{cav}} = \omega_{eg} - \omega_{\text{cav}}$. Transforming the system to the interaction picture and employing the rotating wave approximation, one obtains the Hamiltonian of the system [71]:

$$\begin{aligned}
H &= H_{\text{atom}} + H_{\text{cavity}} + H_{\text{int}} \\
&= -\hbar\left[\Delta_C\sigma_{uu} + \Delta_{\text{cav}}a^\dagger a + g(\sigma_{eg}a + a^\dagger\sigma_{ge}) + \frac{\Omega_c}{2}(\sigma_{eu} + \sigma_{ue})\right].
\end{aligned} \tag{2.3}$$

Here $\sigma_{fi} = |i\rangle\langle f|$ is the population operator of an atomic state in case $i = f$ and couples the atomic states $|i\rangle$ and $|f\rangle$ for $i \neq f$. $a^\dagger$ and a are the creation and annihilation operators of a photon in the cavity, respectively. The combined state of the atom-cavity system is a product state $|x, n\rangle$ with the atomic state $|x\rangle \in \{|g\rangle, |u\rangle, |e\rangle\}$, and $|n\rangle \in \{|0\rangle, |1\rangle, |2\rangle, \dots\}$ representing the number of quanta in the cavity. Restricting ourselves to a subspace with at most one excitation in the cavity ($n = 0, 1$), and choosing the basis
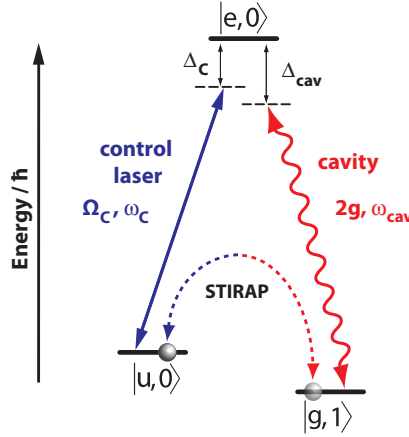
Figure 2.1.: A three-level atom with its states coupled in Λ-configuration by an external laser field and the cavity. The control laser field with frequency ω_c and Rabi frequency Ω_C couples the atomic ground state $|u\rangle$ with the excited state $|e\rangle$. The cavity mode with frequency ω_{cav} and vacuum Rabi frequency $2g$ couples the other ground state $|g\rangle$ with the excited state $|e\rangle$. Δ_C and Δ_{cav} denote the detunings of the laser field and the cavity from the respective atomic transition.

$\{|g, 1\rangle, |u, 0\rangle, |e, 0\rangle\}$, one of the eigenstates of the Hamiltonian we obtain on two-photon resonance ($\Delta_C = \Delta_{\mathrm{cav}} = \Delta$) is [71]

$$|\varphi_0\rangle = \cos\theta\, |u, 0\rangle - \sin\theta\, |g, 1\rangle. \qquad (2.4)$$

This state is a so-called *dark state* since is contains no contribution of the excited state $|e\rangle$, which means that no light can be emitted via spontaneous decay. The relative amplitudes of the states $|u, 0\rangle$ and $|g, 1\rangle$ are determined by the mixing angle

$$\tan\theta = \frac{\Omega_c}{2g}. \qquad (2.5)$$

In the limit of vanishing Rabi frequency of the control laser, $\Omega_c/2g \to 0$, the dark state is identical with state $|u, 0\rangle$. In the other limit of large Rabi frequency $\Omega_c/2g \to \infty$, the dark state corresponds to the state $|g, 1\rangle$ with exactly one photon in the cavity.

The basic idea of the STIRAP is to exploit the dark state and to drive the atom coherently between the two ground states $|u, 0\rangle$ and $|g, 1\rangle$ by varying the mixing angle θ with time. Depending on the starting point, this scheme can be used either to generate photons or to store them.

So far, an idealized system was considered where any kind of dissipation was ignored. Yet, in any real-world experiment, both the atom and the cavity couple to an external reservoir, with rates described by γ and κ, respectively. The excited atomic state $|e\rangle$ decays to the ground states with a rate 2γ. Likewise, the cavity decay leads to dissipation of the excited states $|n\rangle$ to the vacuum state $|0\rangle$ at a rate 2κ. For a successful STIRAP it is therefore crucial that the transfer takes place adiabatically, such that the system will remain in the

dark state at all times. One can show that adiabaticity is given if [71]

$$\frac{g^2}{\gamma} \gg \dot{\theta} + \frac{\kappa}{2}. \tag{2.6}$$

This condition imposes a restriction on how fast the mixing angle θ and thus the control Rabi frequency $\Omega_c(t)$ can be changed in time. If Eq. (2.6) is not satisfied, the dark state φ_0 is no longer an eigenstate of the system at all times, and the excited state $|e\rangle$ can be populated, which in turn can lead to spontaneous emission of a photon into free space.

Photon generation: In order to generate a single photon, one has to initialize the system in state $|u, 0\rangle$, and then transfer it to state $|g, 1\rangle$ via a vacuum-stimulated Raman adiabatic passage (vSTIRAP):

$$|u, 0\rangle \xrightarrow{\Omega_C/2g \to \infty} |g, 1\rangle. \tag{2.7}$$

This creates a single photonic excitation of the cavity field, which, due to the cavity decay κ, is coupled out of the cavity into a well-defined free-space mode, leaving the system in state $|g, 0\rangle$.

Photon storage: Time-reversal of the photon generation process makes it possible to coherently store a single photon impinging onto the cavity in a single atom [70]. This time, the atom is prepared in state $|g\rangle$, and the control field is already switched on with a Rabi-frequency $\Omega_c \gg 2g$ when the photon arrives such that the system is initially in state $|g, 1\rangle$. If now the control field decreases adiabatically, the system will undergo an adiabatic transfer into the state $|u, 0\rangle$

$$|g, 1\rangle \xrightarrow{\Omega_C/2g \to 0} |u, 0\rangle. \tag{2.8}$$

2.1.2. Characterizing entanglement

This section gives a theoretical description of the quantum mechanical phenomenon of entanglement. It will be restricted to bipartite entanglement, i.e. the entanglement of two systems, which is relevant for the experiments presented later in this thesis.

The emergence of entanglement of different systems is closely related to the mathematical concept of separability. Consider two particles A and B with Hilbert spaces $\mathcal{H}_A$ and $\mathcal{H}_B$. A state ρ from the two-particle Hilbert space $\mathcal{H} = \mathcal{H}_A \otimes \mathcal{H}_B$ is called separable if it can be expressed by

$$\rho = \sum_i p_i \rho_i^A \otimes \rho_i^B \tag{2.9}$$

with $\sum_i p_i = 1$ and $p_i \geq 0$ [72, 73]. Here, ρ_i^A and ρ_i^B are density operators that describe single-particle states in their respective Hilbert spaces. If and only if a state ρ is *not* separable, it is called an entangled state.

There exist measures that allow to distinguish entangled from separable states and to quantify to which degree a state is not separable [74, 75]. Some of them, for instance the logarithmic negativity [76], require the experimenter to reconstruct the complete density matrix ρ of the two-particle state by quantum state tomography (see e.g. [77, 78]). To this end, one performs measurements on both particles and correlates the results obtained

in different measurement bases (see e.g. [79, 80]). Applying the respective measure to the density matrix then gives information about the degree of entanglement.

Reconstruction of the density matrix might seem to be the most straight-forward approach, but it has the disadvantage of being experimentally quite cumbersome. In our case of an entangled state of two qubits, the full tomographic reconstruction of the density matrix requires correlation measurements in nine different combinations of bases, and a correspondingly large number of experimental runs. It is reasonable if one is interested in full information on the generated state.

A faster way is to compute the fidelity $\mathcal{F}$, which expresses the overlap of the measured state with an ideal entangled state. For the state most relevant in our experiments, the maximally entangled Bell state $|\Psi^-\rangle = \frac{1}{\sqrt{2}}(|\downarrow\rangle_A |\uparrow\rangle_B - |\uparrow\rangle_A |\downarrow\rangle_B)$ with the qubit basis states $\{|\downarrow\rangle, |\uparrow\rangle\}$, the fidelity is given by

$$\mathcal{F}(|\Psi^-\rangle, \rho) = \langle \Psi^- | \rho | \Psi^- \rangle. \tag{2.10}$$

If the measured fidelity exceeds $50\,\%$, ρ is not separable, and the system is in an entangled state. A priori knowledge of the target state which is ideally prepared can be used to construct a so-called entanglement witness $\mathcal{W}$ which is a Hermitian operator with the two defining properties [73, 81]:

- $\mathrm{Tr}\,[\mathcal{W}\rho] < 0$ if ρ is entangled
- $\mathrm{Tr}\,[\mathcal{W}\rho] \geq 0$ for all separable states.

Using the witness, already a subset of measurements is enough to detect whether the state one actually has prepared is entangled or not. Knowledge of the ideally prepared state is essential for the construction of $\mathcal{W}$, since the condition $\mathrm{Tr}\,[\mathcal{W}\rho] < 0$ is only sufficient to prove entanglement but not necessary, meaning that for a given operator $\mathcal{W}$ entangled states with $\mathrm{Tr}\,[\mathcal{W}\rho] > 0$ may exist.

A suitable entanglement witness operator for the above mentioned $|\Psi^-\rangle$ Bell state is derived in [82, 83, 84]. Its expectation value is

$$\langle \mathcal{W} \rangle = \mathrm{Tr}\,[\mathcal{W}\rho] = \frac{1}{2} \left(p_{|\uparrow_x\uparrow_x\rangle} + p_{|\downarrow_x\downarrow_x\rangle} + p_{|\uparrow_y\uparrow_y\rangle} + p_{|\downarrow_y\downarrow_y\rangle} + p_{|\uparrow_z\uparrow_z\rangle} + p_{|\downarrow_z\downarrow_z\rangle} - 1 \right), \tag{2.11}$$

where $|\downarrow_x\rangle, |\uparrow_x\rangle, |\downarrow_y\rangle, |\uparrow_y\rangle, |\downarrow_z\rangle$, and $|\uparrow_z\rangle$ are the eigenvectors of the Pauli spin matrices. This expectation value can be determined by measuring correlations in only three different, mutually unbiased bases. Here, $p_{|\uparrow_i\uparrow_i\rangle}$, for instance, denotes the probability to measure both qubits in the state $|\uparrow_i\rangle$ if the individual qubits are measured in the basis $\{|\downarrow_i\rangle, |\uparrow_i\rangle\}$.

$\langle \mathcal{W} \rangle$ is related to the fidelity $\mathcal{F}$ via [83]

$$\mathcal{F} = \frac{1}{2} - \langle \mathcal{W} \rangle. \tag{2.12}$$

The described formalism applies to both, atomic and photonic qubits. In the experiments presented in this thesis, the atomic qubits are detected by mapping them onto polarization states of single photons which are subsequently detected in different polarization bases. The atomic spin states on the Bloch sphere and the photonic polarization states on the Poincaré sphere are treated equivalently:

Atomic qubit	Photonic qubit
$\lvert\downarrow_z\rangle$	$\lvert R\rangle$ (right circular)
$\lvert\uparrow_z\rangle$	$\lvert L\rangle$ (left circular)
$\lvert\downarrow_x\rangle = \frac{1}{\sqrt{2}}(\lvert\downarrow_z\rangle + \lvert\uparrow_z\rangle)$	$\lvert H\rangle$ (horizontal)
$\lvert\uparrow_x\rangle = \frac{1}{\sqrt{2}}(\lvert\downarrow_z\rangle - \lvert\uparrow_z\rangle)$	$\lvert V\rangle$ (vertical)
$\lvert\downarrow_y\rangle = \frac{1}{\sqrt{2}}(\lvert\downarrow_z\rangle + i\lvert\uparrow_z\rangle)$	$\lvert D\rangle$ (diagonal)
$\lvert\uparrow_y\rangle = \frac{1}{\sqrt{2}}(\lvert\downarrow_z\rangle - i\lvert\uparrow_z\rangle)$	$\lvert A\rangle$ (antidiagonal)

Therefore, the expectation value $\langle\mathcal{W}\rangle$ can be rewritten for polarization qubit states:

$$\langle\mathcal{W}\rangle = \mathrm{Tr}\left[\mathcal{W}\rho\right] = \frac{1}{2}\left(p_{\lvert H,H\rangle} + p_{\lvert V,V\rangle} + p_{\lvert D,D\rangle} + p_{\lvert A,A\rangle} + p_{\lvert R,R\rangle} + p_{\lvert L,L\rangle} - 1\right). \qquad (2.13)$$

2.2. Experimental setup

The experimental setup of the single atom-cavity quantum node which is at the heart of the experiments described in this thesis has been treated in much detail before [83, 85]. This section will therefore only give a brief overview of the current status of the experiment and of all relevant parameters.

For all the experiments to be described, a single Rubidium atom is trapped at the center of a Fabry-Perot-type cavity characterized by the following parameters (taken from [85]):

$$
\begin{aligned}
\text{mirror transmissions} \quad & T_1 = 2 \pm 0.5\,\mathrm{ppm}, \\
& T_2 = 101 \pm 2\,\mathrm{ppm} \\
\text{radius of curvature} \quad & r = 5\,\mathrm{cm} \\
\text{mirror distance} \quad & l = 495 \pm 2\,\mathrm{\mu m} \\
\text{mode waist} \quad & w = w_{1/e^2} = 30\,\mathrm{\mu m} \\
\text{free spectral range} \quad & FSR = 303 \pm 1\,\mathrm{GHz} \\
\text{cavity decay rate} \quad & \kappa/2\pi = 2.8 \pm 0.1\,\mathrm{MHz} \\
\text{finesse} \quad & F = 56000 \\
\text{round-trip loss} \quad & L_{rt} = 2\pi/F = 113 \pm 2\,\mathrm{ppm} \\
\text{output directionality} \quad & \eta_{out} = 89\,\%
\end{aligned}
$$

The transmission coefficients were chosen asymmetrically on purpose, to ensure that photons inside the cavity will leave preferentially on one side where they can be collected efficiently. Conversely, the mirror with the higher transmission can also be used to efficiently couple single photons from a matching outside mode into the cavity.

Any experimental cycle starts with the preparation of a cloud of cold atoms in a magneto-optical trap (MOT) outside the cavity, see **(a)** in Fig. 2.2. Once enough atoms are loaded, the MOT is switched off and a far-detuned running-wave dipole trap beam **(b)** at 1064 nm with its focus half-way between the region of the MOT and the cavity probabilistically transfers some of the atoms into the cavity **(c)**. There, the atoms are localized in a standing wave trap formed by two counter-propagating dipole trap beams also at 1064 nm collinear with the transfer trap and focussed down to the center of the cavity. The atoms
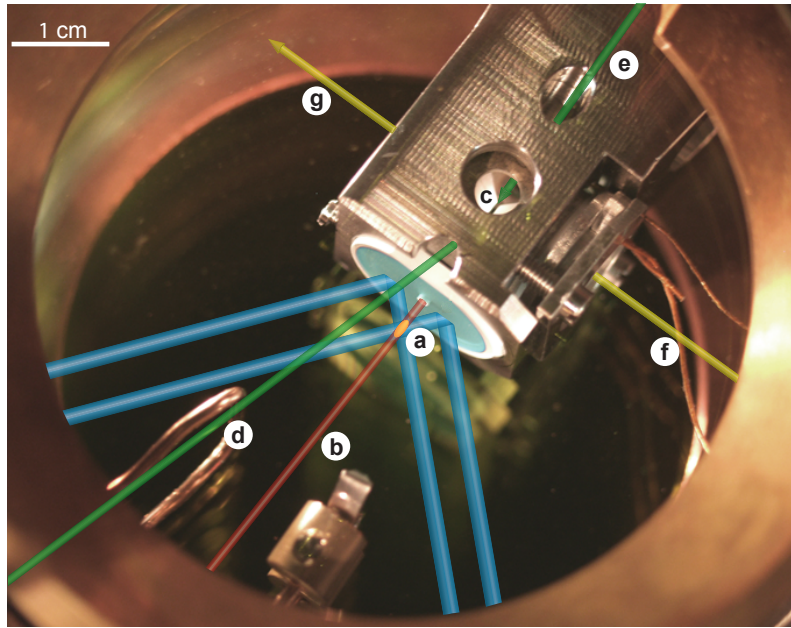
Figure 2.2.: Top view of the vacuum chamber with the cavity. A cloud of cold ^{87}Rb atoms is prepared in a magneto-optical trap (a). A far-detuned dipole trap beam (b) guides some of the atoms into the high-finesse cavity (c). There, the atoms are quasi-permanently trapped in a 1D optical lattice along (b). Various measurement protocols are realized by repeatedly applying laser fields (d) and (e) to the trapped atom. Light can also be coupled into and out of the resonator (f, g). The output mode (g) of the cavity is coupled into a single-mode fiber and directed to a detection setup.

are cooled by transversally applied laser light near-resonant with the light-shifted atoms **(d)**. In a typical measurement sequence, cooling intervals alternate with intervals where an experimental protocol is run, which is typically composed of a series of laser pulses **(d and e)** or microwave pulses (not shown), e. g. for optical pumping and the generation of single photons.

The parameters of the far-detuned standing-wave dipole trap are listed in the following table (partially taken from [85]).

wavelength	1064 nm
Focus size ($1/e^2$ radius)	16 μm
Rayleigh length	0.7 mm
Trap depth at focus	1.5 mK/W
Typical power	1.7-2.2 W

A high numerical aperture objective ($NA = 0.4$) [85, 86] collects photons scattered by the atoms during the cooling periods and directs them onto an EMCCD camera. The spatial resolution of the camera of 1.3 μm does not resolve single anti-nodes of the standing wave. However, analysis of the size and the brightness of the imaged spots allows for the detection of single atoms and for quick reloading in case of atom loss. Based on the image analysis, a glass plate in the beam of the standing wave trap can be tilted to apply a phase shift

that positions the atom at the center of the cavity mode where the coupling is strongest [87].

The number of atoms loaded into the cavity depends on the number of atoms in the MOT, which can be controlled by the MOT duration and the intensity of the cooling and repumping beams of the MOT. Since the loading is probabilistic, ideal settings will lead to successful loading of a single atom in one out of three attempts, assuming poissonian statistics. With trapping times on the order of a minute and a time of only a few seconds to reload a single atom, duty cycles, i.e. the fraction of time where a single atom is present, of around 80 %, have been achieved.

The length of the resonator is actively stabilized using light at 785 nm (until spring 2012) and 770 nm (since then) monitored in transmission. The frequency of the stabilization light is chosen such that it is detuned from the desired frequency of the resonator by an integer multiple, N, of the free spectral range. In case of the 785 nm stabilization light, this was $N = 8$ (D_2 line) and $N = 16$ (D_1 line), and for the light at 770 nm it is $N = 17$ (D_2 line). In all the experiments described in this thesis, the power of the cavity stabilization light and therefore the resulting intra-cavity trapping potential is kept very low. With only a few 10 μK, and considering the temperature of the atoms of ≈ 100 μK, it is negligible compared to the mK trapping potential of the far-detuned trap.

A bandpass-filter is used to separate the cavity stabilization light from the signal photons at 780 (795) nm which are efficiently coupled into a single-mode optical fiber and sent to a detection setup consisting of two or more single photon counting modules. A combination of waveplates and a polarizing beam splitter allows us to perform measurements in alternating polarization bases. For the experiments described in the following, the efficiency to detect a single photon after leaving the cavity through the out-coupling mirror ranged from 18 % to 44 %, mainly limited by the quantum efficiency of the single photon counters $(0.5 - 0.6)$ and the coupling efficiency of the free-space mode into the single-mode fiber (up to 0.85).

For the experimentally relevant atomic transitions $5^2S_{1/2} \, |F = 1\rangle \leftrightarrow 5^2P_{3/2} \, |F = 1\rangle$ (D_2 line, 780 nm) and $5^2S_{1/2} \, |F = 1\rangle \leftrightarrow 5^2P_{1/2} \, |F = 1\rangle$ (D_1 line, 795 nm), the maximum achievable atom-cavity coupling is $g_0 = 2\pi \cdot 5.1$ MHz (D_2 line) and $g_0 = 2\pi \cdot 2.3$ MHz (D_1 line), respectively. Since the atom is not strongly confined along the cavity axis, it can move over several nodes and anti-nodes of the cavity field, which makes the atom-cavity coupling fluctuate over time and leads to an effective coupling of $g_{\text{eff}} \approx g_0/2$.

The losses of the system are described by the decay of the cavity field $\kappa = 2\pi \cdot 2.8$ MHz, which is dominated by output coupling of the field through the mirror with the higher transmission, and the polarization decay rate of the excited atomic state $\gamma = 2\pi \cdot 3$ MHz. For the D_2 line, this puts our system in the intermediate coupling regime with a maximum cooperativity of $C = g_0^2/2\kappa\gamma \approx 1.5$. For the D_1 line with a cooperativity of $C \approx 0.3$, we operate in the weak to intermediate coupling regime.
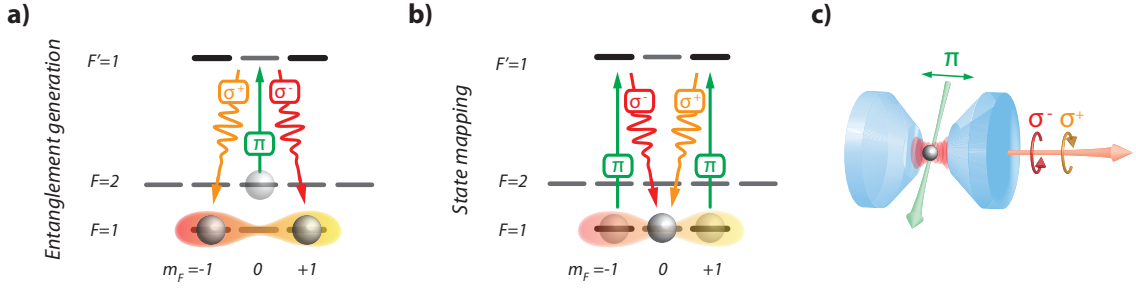
Figure 2.3.: Entanglement scheme. (a) The two possible paths of the photon generation process lead to entanglement between the polarization of the photon and the Zeeman state of the atom. **(b)** The atomic state is mapped onto the polarization of a second photon. **(c)** Polarization components as seen in the laboratory frame of reference.

2.3. Generation of atom-photon entanglement

The generation of single photons via the vacuum stimulated Raman adiabatic passage introduced in Sec. 2.1.1 is a powerful tool. Not only is our atom-cavity system one of the most efficient on-demand photon sources [88, 89], the vSTIRAP also gives us control over a number of important parameters of the emitted photons.

The temporal envelope of the control Rabi frequency Ω_C directly controls the temporal envelope of the photonic wave packet, allowing for photons shorter or longer in time, and, in principle, with arbitrary shape, merely restricted by the finite κ and the adiabaticity criterion, Eq. (2.6) [90, 91]. The detuning Δ determines the frequency of the photons [92]. By changing Δ, we can tune the frequency over several tens of MHz with almost no effect on the photon generation efficiency [89], which is essential when connecting systems that require slightly different frequencies, e.g. two single atoms, or a single atom and a BEC in traps causing different a.c. Stark shifts, as discussed in chapter 3. Selective coupling of the control laser and the cavity to certain spin-states of the atom leads to pre-defined polarizations of the emitted photons [93, 94] and, moreover, can even be used to map the internal state of the atom onto the polarization of a single photon [70, 95]. However, for quantum information applications, one of the most striking features is the possibility to create entanglement between the spin state of the atom and the polarization degree of freedom of a single emitted photon [14, 96].

To this end, the $5^2S_{1/2}$ hyperfine ground states $F = 1$ and $F = 2$ of the atom are coupled in the Λ configuration described in Sec. 2.1.1. The cavity is near-resonant with the $F = 1 \leftrightarrow F' = 1$ transition of the D_2-line (D_1-line), and the control laser is on two-photon resonance ($\Delta_C = \Delta_{\mathrm{cav}} = \Delta$) with the cavity and couples the respective $F = 2 \leftrightarrow F' = 1$ transition. To understand the principle of the entanglement protocol, the simple three-level scheme described in Sec. 2.1.1 needs to be extended to the configuration shown in Fig. 2.3 **(a)** and **(b)**, where the internal level structure of the atom is considered.

The atom is initially prepared in state $|F = 2, m_F = 0\rangle$ by optical pumping, as will be explained in Sec. 3.1.3. With the cavity axis chosen to be the quantization axis, the π-polarized control laser beam (see Fig. 2.3) couples this state to $|F' = 1, m_F = 0\rangle$, and

increasing the control Rabi frequency Ω_C drives an adiabatic passage resulting in the emission of a single photon from the cavity. This passage can happen via two paths that are equally likely and indistinguishable, see Fig. 2.3 (**a**). The first is the transfer of the atom into the state $|1, -1\rangle$, accompanied by the emission of a $|\sigma^+\rangle$ photon, the second brings the atom into state $|1, +1\rangle$ while a $|\sigma^-\rangle$ photon is emitted. The result is a superposition of the two possible paths, which leaves the system in the maximally entangled Bell state

$$\left|\Psi^-_{\text{atom}\otimes\text{photon}}\right\rangle = \frac{1}{\sqrt{2}}\left(|1, -1\rangle\left|\sigma^+\right\rangle - |1, +1\rangle\left|\sigma^-\right\rangle\right), \tag{2.14}$$

with the relative phase between the terms given by the Clebsch-Gordan coefficients of the atomic transitions involved. The photon can either be sent to a detection setup where its polarization is projected, thereby also projecting the atomic state. Alternatively, a the photon and the information it carries can be transmitted to another node in a quantum network. The latter is discussed in detail in Sec. 3, but for now let us assume the photon is immediately detected.

To verify the entanglement, the atomic state is subsequently mapped onto the polarization of a second photon, see Fig. 2.3 (**b**), by another π-polarized pulse from the control laser, this time coupling the states $|1, \pm1\rangle \leftrightarrow |1', \pm1\rangle$. With this step, the atom-photon entanglement is turned into an entangled state of the two photons

$$\left|\Psi^-_{\text{photon}_2\otimes\text{photon}_1}\right\rangle = \frac{1}{\sqrt{2}}\left(\left|\sigma^-\right\rangle_2\left|\sigma^+\right\rangle_1 - \left|\sigma^+\right\rangle_2\left|\sigma^-\right\rangle_1\right). \tag{2.15}$$

Both photons are guided to the detection setup, where correlation measurements in different polarization bases are taken.

Two figures of merit can be given for our implementation of the generation of atom-photon entanglement and its mapping onto photon-photon entanglement. The first is the generation efficiency, which depends on the parameters of the system, κ, γ, g, and therefore the transition strength of the used atomic transition, and which is largely influenced by the temporal amplitude of the control field and the frequency detuning Δ [89]. The maximum reachable efficiency of photon generation on the D_1 line with a $g_0 = 2.3\,\text{MHz}$ is smaller than on the D_2 line with a $g_0 = 5.1\,\text{MHz}$, because of the smaller g and thus a more likely admixture of the excited state $|e\rangle$ during any adiabatic passage, which is the reason why all the early experiments in our group focused on the generation of photons on the D_2 line [71, 79, 80, 86, 97]. Comparison of the single photon generation efficiency on both transitions with one and the same system shows that efficiencies of up to $34\,\%$ on the D_1-line and $56\,\%$ on the D_2-line can be achieved [89]. The efficiencies cited here refer to the efficiency of generating a single photon into the mode of the cavity, $89\,\%$ of which will leave the cavity through the outcoupling mirror. The second figure of merit is the fidelity of the entangled state created. Since we are not able to read out the atomic state directly, but can only map it onto the polarization of a second photon, we can solely make a statement on the fidelity of the two-photon entangled state given in Eq. (2.15).

If the scheme is realized exactly like depicted in Fig. 2.3, one expects perfect overlap of the created state with the $|\Psi^-\rangle$ Bell state. However, in the actual experiment there are several detrimental effects that lead to a reduction of the fidelity. As will be shown below, these effects are stronger on the D_2 line than on the D_1 line, and to understand why, it
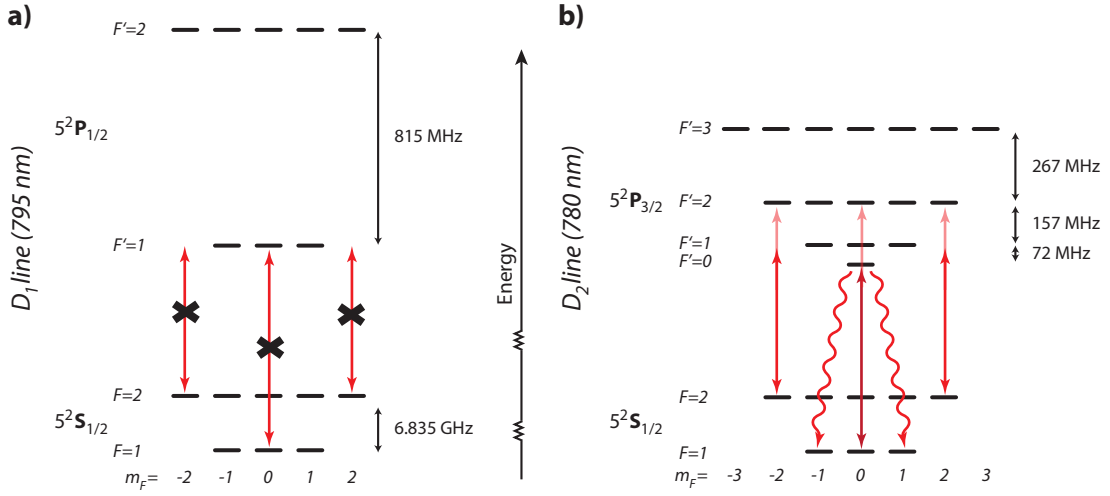
Figure 2.4.: Comparison of the level schemes of the D_1 and D_2 line. a) On the D_1 line, off-resonant excitations are suppressed by the large level spacing. Population in state $|1,0\rangle$ cannot be transferred by the π-polarized control-beam due to selection rules. **b)** The level spacing of the excited state manifold of the D_2 line is much smaller, increasing the probability to excite off-resonant transitions via the $F' = 0$ and $F' = 2$ states. The spacing between the levels of the excited state manifolds is to scale. Note that the depicted level scheme is the one of the free atom, and that light shifts due to the dipole trap have been neglected.

is necessary to take the entire excited state manifolds of the two lines into consideration. Fig. 2.4 contrasts the two manifolds to illustrate their benefits and possible problems. For the D_1 line, there exists only one other excited state, the $|F' = 2\rangle$ state, which is, with 815 MHz, quite far detuned from the $|F' = 1\rangle$ state used in the entanglement protocol. The D_2 line on the other hand comprises three other exited states with detunings from the $F' = 1$ state of 72 MHz ($F' = 0$), 157 MHz ($F' = 2$), and 267 MHz ($F' = 3$), respectively [98].

Ideally, the protocol starts by initializing the atom in the state $|F = 2, m_F = 0\rangle$. In case of imperfect optical pumping, however, some population may remain in the Zeeman states $|F = 2, m_F = \pm2\rangle$ and $|F = 2, m_F = \pm1\rangle$.

For the D_1 line, off-resonant coupling of the outer states with $m_F = \pm2$ to the excited $F' = 2$ is very unlikely due to the large detuning, so these states do not contribute to any photon generation process. Coupling of the π-polarized control laser pulse to population in the $m_F = \pm1$ states will lead to photon emission, however, the resulting state is not the one from Eq. (2.14) but one that leaves the atom in the state $|1,0\rangle$. Since the $|1,0\rangle \leftrightarrow |1',0\rangle$ transition is dipole-forbidden, the attempt to map the atomic state onto the polarization of a second photon by applying another control laser pulse will not lead to the emission of a photon. Detection of the mapping photon, therefore, indicates a successful entanglement event, and improved optical pumping will affect only the efficiency of the overall process.

On the D_2 line, the outer states with $m_F = \pm2$ should still have a negligible influence if the detuning is set such that off-resonant excitation of the $|F' = 2, m_F = \pm2\rangle$ states is very improbable. Like on the D_1 line, population in $m_F = \pm1$ will generate a photon, and

the atom will end up in $|1,0\rangle$. Unlike on the D_1 line, however, applying a control pulse to map the atomic state onto a second photon can here lead to the subsequent generation of photons via off-resonant excitation of the states $|0,0\rangle'$ or $|2,0\rangle'$ after the STIRAP is finished. If such an excitation event results in the transfer of the atom into Zeeman states $|1,\pm1\rangle$, this can lead to yet another photon being emitted into the cavity, transferring the atom back into the state $|1,0\rangle$ where the cycle begins again as long as the control laser beam is still switched on and the atom is not lost to state $F=2$, giving rise to a train of photons coming out of the cavity. The same holds for the case of perfect optical pumping, where the two steps of entanglement generation and mapping of the atomic state onto a photon end with the atom in state $|1,0\rangle$. The only ways to circumvent or to at least abate this problem of off-resonant excitation is to choose a detuning Δ that is as far away from the excited $F'=0$ and $F'=2$ states as possible, and to use a weak read-out pulse. Post-selection on the arrival time of the detected mapping photon can further increase the fidelity, since photons generated after off-resonant repumping will reach the detector later in time than photons created in the desired way. All these considerations played a role when searching for the optimal parameters of the experiments described in Sec. 3. In contrast to the D_1 line, where off-resonant excitation is not a problem, one faces a trade-off on the D_2 line between a high fidelity on one side and the efficient read-out of the atomic state by mapping it onto another photon on the other.

The following table lists typical values from the experiment, cf. [89, 95, 99, 100].

	D_1 **line**	D_2 **line**
detuning Δ from the light-shifted $\|2,0\rangle \leftrightarrow \|1,0\rangle'$ transition	0, i.e. on resonance	43 MHz blue-detuned
efficiency of generating a 1st photon	34 %	45 %
conditional efficiency of generating a 2nd photon	30 % [83]	3 %*
efficiency of generating an entangled photon-pair	10 %	1 %*
maximum fidelity with Ψ^-	96 %	94 %*

Table 2.1.: Typical efficiencies of the entanglement generation protocol on the D_1 and D_2 line.
*Note compromise: A stronger read-out pulse improves the efficiency of generating a second photon to e.g. 15 % but at the same time leads to a decrease of the fidelity to 85 %.

Another deviation from the perfect scheme are circular components of the ideally π-polarized control beam, which in a real-world experiment can only be minimized but never be entirely precluded. These components will lead to coupling between states other than the ones desired in the entanglement scheme and can lead to the generation of photons on unintended transitions. Since these circular contributions are small compared to the π-polarized components, any adiabatic passage or off-resonant excitation caused by them will take place on a slower time scale, such that again post-selection on the arrival time of the detected photons is a valid means to characterize the fidelity of the initial
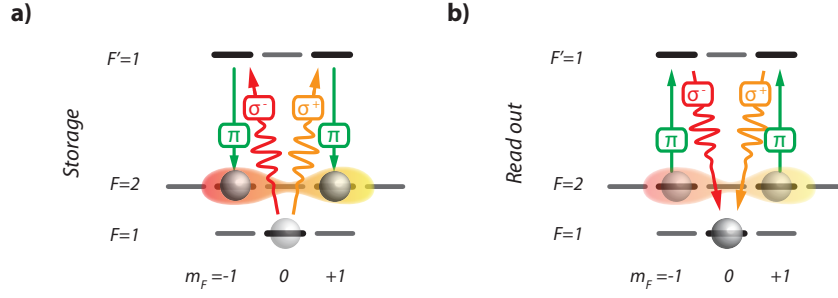
Figure 2.5.: Storage scheme. a) A single photon is coherently stored in the atom, and a qubit encoded in its polarization is mapped onto a superposition of the $|F = 2, m_F = \pm 1\rangle$ states of the atom. **b)** The stored qubit is retrieved when a read-out pulse maps the atomic state back onto the polarization state of a photon.

atom-photon entangled state.

2.4. Storage of single photons in a single-atom quantum memory

So far in this chapter, the capabilities of an atom-cavity node to create single photons and to generate entanglement between a single atom and a single photon have been demonstrated. The other key ingredient for future quantum network applications is the ability to recieve, faithfully store and re-send quantum information. In the following, I explicate how this task, the storage and retrieval of a qubit encoded in the polarization of a single photon, can be achieved with a single atom in a cavity.

In Section 2.1.1, the coherent mapping of a single photon onto a single atom by means of an adiabatic passage was described. Again, the cavity and the control laser are on two-photon resonance, with both the cavity and a photon to be stored near-resonant with the $F = 1 \leftrightarrow F' = 1$ transition, and the control laser coupling the $F = 2 \leftrightarrow F' = 1$ transition. To map not only a photonic excitation but also a polarization qubit onto the atom, it is again necessary to extend the simple three-level scheme to the more complicated double Λ-scheme familiar from section 2.3. The implementation of the storage scheme is illustrated in Fig. 2.5.

Initially, the atom is prepared in state $|F = 1, m_F = 0\rangle$, and a π-polarized control beam with Rabi frequency $\Omega_C \gg 2g$ couples the states $|2, \pm 1\rangle \leftrightarrow |1', \pm 1\rangle$, as illustrated in Fig. 2.5 (**a**). Choosing the cavity axis as the quantization axis, a photon impinging onto the cavity carries a qubit encoded in a superposition of σ^+ and σ^- polarization:

$$|\psi_{\text{photon}}\rangle = \alpha \left|\sigma^-\right\rangle + \beta \left|\sigma^+\right\rangle \tag{2.16}$$

with complex amplitudes α and β, and the normalization $|\alpha|^2 + |\beta|^2 = 1$. The $\sigma^\pm$ component of the polarization couples the atomic states $|1, 0\rangle \leftrightarrow |1', \pm 1\rangle$. According to Eq. (2.8), an adiabatic decrease of the control Rabi frequency $\Omega_C(t)$ upon arrival of the photon coherently stores it in the atom, thereby mapping the polarization components of the photon

onto internal states of the atom, see Fig. 2.5 (**a**):

$$\alpha \left| \sigma^- \right\rangle + \beta \left| \sigma^+ \right\rangle \longrightarrow \alpha \left| 2, -1 \right\rangle + \beta \left| 2, +1 \right\rangle. \tag{2.17}$$

The two pathways of storing σ^-- and σ^+-polarized photons are indistuingishable, thus no information about the incident polarization is gained, and the state itself and especially the phase of the superposition state is preserved.

After a variable storage time, the qubit can be retrieved by mapping it back onto a photon. This is done by increasing the Rabi frequency of the control laser and thus driving a vSTIRAP as illustrated in Fig. 2.5 (**b**). Thereby, the atomic superposition state is reconverted into the superposition state of the polarization components of the created photon from Eq. (2.16).

Apart from some characteristics like the optimum frequency, the acceptance bandwidths and the storage time, which are inherent to our implementation, the single-atom quantum memory is characterized by two figures of merit, the efficiency of the combined storage-and-retrieval process, and the fidelity with which a quantum state can be written into and read out of the memory. In the first realization of such a single-atom quantum memory [70, 101], coherent pulses attenuated down to the single-photon level were used to characterize the memory. Preparing the measurements of chapter 3, the characterization measurements were repeated with true single photons provided by the second atom-cavity system. Since a detailed description of the modus operandi of these measurements is given in [78], I will only summarize the results also published in [78, 95].

The efficiency of the memory is determined by comparing the number of retrieved photons with the number of reference photons. The latter impinge onto the cavity, enter the resonator, and experience losses due to absorption and transmission through the high-reflector before they leave the cavity again through the output-coupler with an experimentally determined probability [78]. Since transmission losses on the way from the cavity to the detectors are equal for both retrieved photons and reference photons, this allows to calculate the probability of a single photon in front of the cavity to be stored, retrieved, and to leave the cavity through the high-transmissive mirror.

Averaging over 12 hours of data taking, the combined write-read efficiency we obtained after a storage time of $2.5\,\mu s$ was $(10 \pm 1)\,\%$ [95].

The fidelity is investigated by performing quantum process tomography on the single-atom quantum memory, as described in [78, 101]. For this tomography, we set the polarization of the incoming photon and compare it to that of the retrieved photon after storage. With respect to a set of ideal input states, we measure the average fidelity to be $\bar{\mathcal{F}} = (92.2 \pm 0.4)\,\%$ [95], clearly exceeding the value of 2/3 achievable by a classical intercept and resend method [102].

This value corresponds well to the fidelity obtained in the first demonstration of the single-atom quantum memory characterized with weak laser pulses, where an average fidelity of 93 % was observed [70, 101], but is significantly lower than the up to 98 % fidelity reached after optimizing the process of optical pumping [78]. The difference of about five percentage points can be explained by the relatively low rate of detected photons after retrieval from the memory when characterizing it with true single photons. The low rate is a result of the success probabilities of the individual steps of the protocol, including

single-photon generation, transmission of the single photon from one cavity to the other, storage and retrieval of the photon, and finally its detection by a single-photon counter. This rate needs to be compared to detection events due to imperfect optical pumping into $F = 1$ and to dark-counts of the detectors, both leading to retrieved photons even when no input pulse is present. The ratio of these detrimental events relative to events resulting from successful storage and retrieval is measured to be $1 : 10$. Assuming that the detrimental events are randomly polarized, this explains the observed difference in fidelity between the measurements with single photons as compared to weak coherent pulses [78].

Limiting factors for the fidelity are the non-perfect preparation of the intial state $|1, 0\rangle$ due to off-resonant excitations of the excited $F' = 0$ and $F' = 2$ states of the D_2 line, and again circular components of the ideally π-polarized laser beams, both leading to deviations from the scheme shown in Fig. 2.5. Both effects can result in preparation of the atom in the states $|1, \pm 1\rangle$. While for perfect state preparation in $|1, 0\rangle$ and ideal storage, the atom is transferred into a superposition of the states $|2, \pm 1\rangle$, starting in the wrong state can in turn lead to population of the other Zeeman states of the $F = 2$ manifold. The polarization of photons retrieved from these states is in general not correlated with the polarization of the stored photons. Since the transition strength of the control field depends on the quantum number m_F, the dynamics of the photon emission process depend on the atomic state. Numerical simulations [78] show that photons emitted from the states $|2, 0\rangle$ and $|2, \pm 2\rangle$ have a delay compared to photons retrieved from the the states $|2, \pm 1\rangle$. Like in section 2.3, postselection on early arrival times of the read-out photons can therefore filter out events in which the atom underwent unwanted transitions.

2.5. Storage with many atoms in a cavity

The maximum efficiency of our cavity-based quantum memory predicted by theory [103] scales with

$$\eta_{\mathrm{max,th}} = \frac{C}{1 + C} \ ,$$

(2.18)

where C is the cooperativity parameter. Any gain in atom-cavity coupling should therefore lead to higher efficiencies.

While the coupling strength g for a single atom could be increased significantly by modifying the setup and switching to a cavity with a smaller mode volume, the most obvious way to boost the coupling in the current setup is to work not with just a single atom but with an ensemble of N atoms. Thereby, one can exploit the collective enhancement of the coupling, scaling as $\sqrt{N}g$. This enhancement should lead to higher efficiencies of the storage and retrieval processes, however at the cost of fidelity, since contributions of irregular read-out events due to imperfect optical pumping scale linearly with the number of atoms, which is stronger than the expected increase in efficiency with N. Since $C \propto N$, the efficiency saturates for large N.

According to the Eq. (2.18), working with 10 to 15 atoms instead of a single one could already push the predicted maximum efficiency from around $50\,\%$ to higher than $90\,\%$. Even though the write-read efficiencies that we have demonstrated so far with a single atom are systematically lower than the predicted maximum, one should still expect that

increasing the atom number leads to a significant improvement.

While the storage scheme is in principle the same as in the single atom case, some effects are much more pronounced due to the collective coupling. One is the normal-mode splitting that results from the larger coupling strength, leading to the cavity becoming intransparent on resonance and in turn to the reflection of the pulse one wants to store. The presence of the control beam renders the cavity transparent again due to electromagnetically induced transparency (EIT) [104]. As the linewidth of the EIT window is proportional to Ω_c^2 for a fixed value of $\sqrt{N}g$, one obtains a lower limit for the control Rabi frequency Ω_c for incoming pulses with a certain spectral width. At the same time the group velocity of the pulse inside the cavity grows with Ω_c as $v_{gr} = c/(1 + \frac{2Ng^2}{\Omega_c^2})$ [83], which constitutes an upper limit for Ω_c, since we need to ramp the control beam down adiabatically before the pulse or a too large part of it leaves the cavity again. As we are, at least at this point, not able to reliably and reproducibly prepare an ensemble with a fixed atom number, and since the coupling strength depends not only on the number of atoms but also on their position relative to the cavity mode, finding optimal parameters is challenging.

Investigating the write-read efficiency of our ensemble memory, it turns out that collective effects, while being a virtue on the one hand, become a limiting factor on the other. For simplicity, consider an atomic ensemble in free space, where all atoms are initially prepared in state $|1\rangle$. When storing a single photon (or a weak coherent pulse), the population is brought into a coherent superposition expressed by the Dicke state

$$|D(t=0)\rangle = \frac{1}{\sqrt{N}} \sum_j \exp(i\boldsymbol{k}_{rec}\boldsymbol{r}_j) |1_1 \dots 2_j \dots 1_N\rangle. \qquad (2.19)$$

During the storage process, the j-th atom is transferred from state $|1\rangle$ into state $|2\rangle$ and picks up a differential recoil, resulting in the position-dependent phase factor $\exp(i\boldsymbol{k}_{rec}\boldsymbol{r}_j)$. The differential recoil $\boldsymbol{k}_{rec}$ is acquired by the absorption of the storage photon and the emission of a photon into the control beam.

In the time between storage and read-out, motion of the atoms leads to a change of relative phases between the constituents of the Dicke state and to dephasing, since the motion is thermal and therefore random. As the light of the read-out pulse couples only to the state $|D(t=0)\rangle$, the dephasing of this state results in a time-dependence of the write-read efficiency that is determined by the number of atoms, their temperature, and the exact geometry of the system.

In our current implementation, see Fig. 2.6, the atoms are trapped in a 1D optical lattice, where they are strongly confined only along the direction of the trapping beam (x), whereas their confinement along the two orthogonal axes y and z is weak and allows them to move by several µm. The influence of the cavity stabilization light and the resulting blue-detuned standing wave along the cavity mode is negligible. The control beam is perpendicular to the cavity mode that carries the storage photon, and it intersects the axis of our 1D optical lattice under a 45° angle. Thus, photons from the control beam have momentum components both along a tightly and a weakly confined axis of the dipole trap, x and z, respectively. A photon in the cavity mode on the other hand has a momentum component[1] only along the second weakly confined axis y. During the storage process, a differential

---

[1]The cavity mode function is proportional to $\cos(ky)$, and is a coherent superposition of momenta k_y
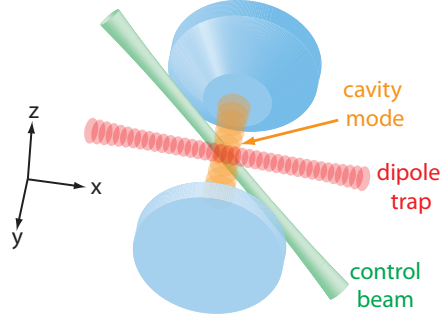
Figure 2.6.: Illustration of the geometry. Photons in the control beam (green) have momentum components both along a strongly (x) and a weakly confined axis (z) of the dipole trap (red). The cavity axis is parallel to a weakly confined axis (y).

recoil is acquired by the absorption of the storage photon and the emission of a photon into the control beam. The recoil has therefore two possible directions, $\boldsymbol{k}_{rec} = \pm\boldsymbol{k}_{ph} - \boldsymbol{k}_c$, and the wavelengths of the created spin wave is $\approx 780\,\text{nm}/\sqrt{2}$.

On the timescales relevant for our experiments, the atoms move by distances comparable to and larger than this, so it becomes clear that dephasing due to thermal motion is the limiting factor in our ensemble approach. At a temperature of around 100 µK [85] and with trap frequencies of 9 kHz for the weakly confined axes, an atom needs on average 5.6 µs to move $780\,\text{nm}/\sqrt{2}$.

A simplified theoretical model, where our trapping potential and the presence of the cavity are neglected, is derived in appendix A. It predicts a Gaussian decay of the write-read efficiency η_{wr} with a time-independent offset:

$$\langle\eta_{wr}\rangle_{avg} = \eta_0\Big(\frac{1}{N} + \frac{N^2 - N}{N^2}\exp(-t^2/\tau^2)\Big), \tag{2.20}$$

where η_0 accounts for finite storage efficiency at $t = 0$ and τ is a function of the temperature. Due to the $1/N$ term, the efficiency will not go down to zero for long storage times but to a constant level determined both by the exact number of atoms and the finite efficiency at $t = 0$.

Despite the simplifications made, this prediction corresponds well to our observations in the experiment. Figure 2.7 **a)** shows a fit of Eq. (2.20) to our data, obtained with the starting time $t = 0$ as the only fixed parameter, set to coincide with the beginning of the incoming pulse at 0.5 µs, see Fig. 2.7 **b)**. The reduced χ^2 of the fit is 12 and lies far outside the 95 % confidence interval, $\chi^2_{red} \in [0, 1.8]$, so its predictions should be taken with a grain of salt. According to the fit, the maximum write-read efficiency is $\eta_0 = 72 \pm 10\,\%$, however at storage times impossible to realize. The atom number obtained from the fit, 12.2 ± 1.4, is realistic, whereas the calculated temperature of 23 ± 2 µK is only a quarter of what we expect from the spatial position spread of the atoms on the camera images [85], clearly indicating that the model is too simplistic.

---

and $-k_y$. The differential recoil is a corresponding superposition. However, only the length of $\boldsymbol{k}_{rec}$ is relevant for the dephasing observed here, so this superposition has no effect.
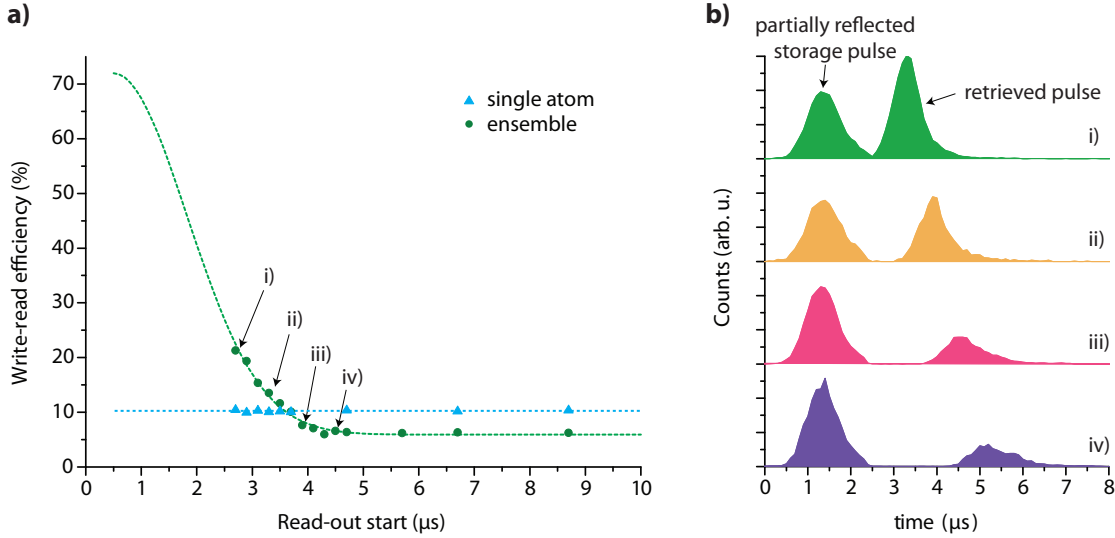
Figure 2.7.: Comparison of photon storage in a single atom and in an ensemble of 10–15 atoms: a) A weak coherent pulse containing an average photon number of 0.5 is stored, and the time between storage and read-out is varied. The write-read efficiency in the single-atom measurement (blue triangles) shows no dependence on the storage time on the timescales we investigated, whereas a strong time dependence is observed in the ensemble case (green dots). The statistical error corresponds to the size of the symbols. Read-out events due to imperfect optical pumping contribute less than absolute 0.3 % in each data set. The green line is a fit of Eq. (2.20). The blue line is a linear fit. **b)** For some of the data points, the corresponding arrival-time distribution of the partially reflected storage pulse and the retrieved pulse is shown.

The estimated and observed dephasing time is on the order of only a few µs. Thus, it is not much longer than both the temporal width of the pulses we store, and also of the retrieved photons, see Fig. 2.7 **b)**. Therefore, non-negligible dephasing occurs already during the write process and possibly still during the read-out. However, a more detailed experimental investigation using significantly shorter pulses is problematic because of the increase in bandwidth of the incoming pulse and the requirement of adiabaticity for the read-out.

Nevertheless, for very short storage times, we observe a write-read efficiency with the atomic ensemble of up to $(21.3 \pm 0.2)\,\%$, which is almost twice as high as that of the single-atom quantum memory. By impeding or slowing down the dephasing, even much higher efficiencies at considerably longer storage times should come into reach [105]. One solution could be to cool the atoms to much lower temperatures. The other is to confine the atoms more strongly along the direction of the differential recoil. A different geometry with the control beam applied along the standing wave trap (in x direction) and using a strong intra-cavity trap, leading to a 2D optical lattice, could possibly overcome our problem. With the current geometry, the Dicke state could be kept from dephasing by strongly confining the atoms in a 3D optical lattice [106].

3. Remote matter-matter entanglement

The previous chapter demonstrated that a single atom coupled to an optical cavity fulfills all the requirements posed to a fully functional network node. In this chapter, two such nodes are combined to form the prototype of an elementary quantum network. Quantum connectivity is achieved by the optical interactions of single atoms and single photons, enabling the distribution of entanglement between the two network nodes by the exchange of just a single photon.

The description of the experimental setup and protocol, and the discussion of the results of the entanglement of two single atoms constitute the main part of this chapter. In the remainder, a comparison is drawn to another experiment in which remote entanglement is created between a single atom and Bose-Einstein condensate in a hybrid quantum network.

3.1. Entanglement of two single atoms at a distance

This section presents one of several experiments carried out in a close and fruitful collaboration of two independently operated atom-cavity experiments at MPQ, one located in the *Photon Pistol Lab*, referred to as node A, and the other, node B, based in the *QGate Lab*.

While I have endeavored to give a self-contained account of these joined experiments, I occasionally take the liberty of omitting experimental details, especially those of the coupling of the two systems, that are covered in depth in the complementary dissertation of my colleague Christian Nölleke [78].

The content of this section has been partially published in
An elementary quantum network of single atoms in optical cavities.
S. Ritter, C. Nölleke, C. Hahn, A. Reiserer, A. Neuzner, M. Uphoff, M. Mücke, E. Figueroa, J. Bochmann, and G. Rempe, *Nature* **484**, 195 (2012)

3.1.1. Connecting the network nodes

The two atom-cavity experiments are run independently, but they share a common clock (a 10 MHz signal from a hydrogen maser by courtesy of the Hänsch group), and light from an optical frequency comb (Menlo Systems FC1550) as references, plus some classical communication channels.

In each of the two laboratories, an FPGA-based digital pattern generator controls the timing of the various steps of the protocol, and the data recording of the single photon detectors. Any jitter between the digital pulses within a sequence is small compared to temporal resolution of the detection system of 2 ns. Relative accuracy between the

experimental runs in the two systems is ensured by working in a master-slave configuration where one systems triggers the other.

The experiments are optically connected by a 60 m long single-mode fiber with anti-reflection coated end-facets. Along the path from atom A to atom B, photons will experience a change in polarization as the fiber and some of the optical components are birefringent. However, these unwanted polarization rotations can be compensated for, since the overall change in polarization is a unitary transformation which can easily be counteracted using waveplates. The details of our polarization compensation are explicated in [78].
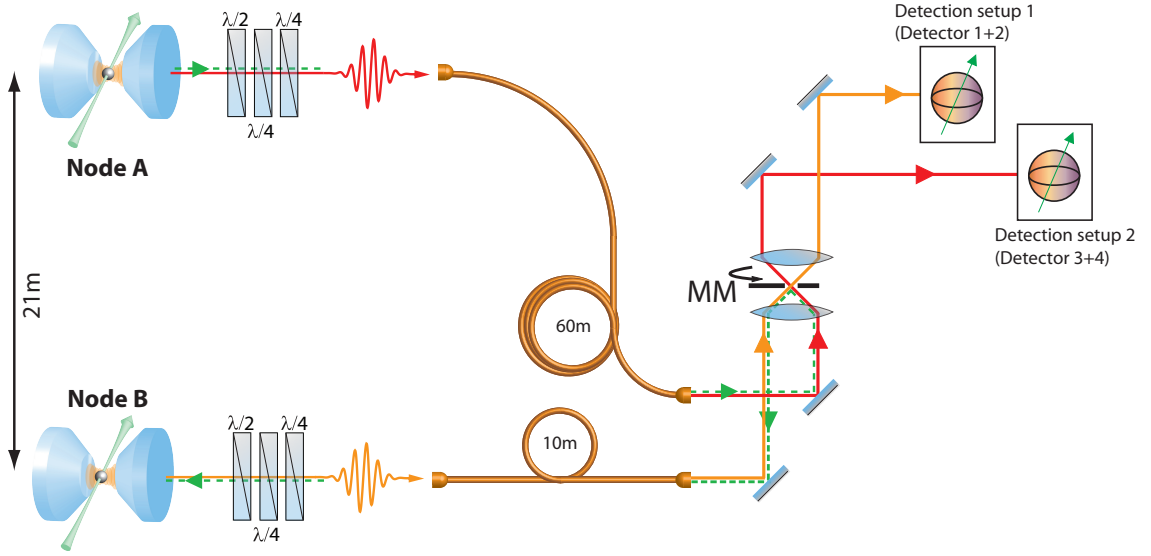
3.1.2. Experimental setup

A direct comparison of the parameters of the two atom-cavity systems at nodes A and B is given in [78]. For all pratical purposes, the two systems can be considered identical. Figure 3.1 shows a sketch of the two systems in the configuration used to create and verify remote entanglement. The waveplates compensating unwanted polarization rotations are set such that, first, the polarization behind the cavity at node A matches the polarization in front of the cavity at node B, and second, that the polarization behind each cavity is identical with the polarization in front of the respective detection setup. A fast-moving mirror is implemented that switches between two configurations. In the first setting, it couples the two atom-cavity nodes and thus directs photons generated at node A to node B, in the other it connects both cavities with their respective detection setup. A detailed description of this mirror, a commercially available computer hard drive modified to meet our requirements is given in [78, 107].

In both laboratories, the control laser and the cavity are on two-photon resonance, $\Delta_C = \Delta_{cav} = \Delta$, at a detuning of $\Delta = 170\,\text{MHz}$ from the transition of the free atom. The a.c. Stark shifts of the relevant transitions were measured to be 120 MHz ($|2, 0\rangle \leftrightarrow |1', 0\rangle$) at node A, and 150 MHz ($|2, \pm1\rangle \leftrightarrow |1', \pm1\rangle$) at node B, respectively. The effective detuning of control laser and cavity from the atom is therefore 50 MHz (node A) and 20 MHz (node B). The difference stems from slightly different trap depths of the far-detuned optical dipole traps which in turn result in different a.c. Stark shifts of the atoms in the two setups.

3.1.3. Experimental protocol

In this section, a step-by-step account is given of the experimental protocol for the generation of remote atom-atom entanglement, see Fig. 3.2.

Any experimental sequence starts with the probabilistic loading of a single atom from the MOT into each of the two cavities. Once a single atom is present at both nodes, the protocol is started and repeated until one of the atoms is lost.

Figure 3.1.: Experimental setup used to create entanglement of single atoms at a distance. A single photon (dashed green line) entangled with the atom at node A is transmitted to the cavity at node B and coherently stored in the atom there. To verify the entanglement, the atomic states on both sides are mapped onto the polarization of single photons (red and yellow lines) which are evaluated by two independent detection setups 1 and 2. Waveplates ($\lambda/2$, $\lambda/4$) are used to compensate for unwanted polarization rotations. MM is a fast-moving mirror that reflects the entangled photons from node A to node B and transmits the read-out photons from both cavities to the respective detection setups. Adapted with minor changes from [78].

Optical pumping at nodes A and B

The protocol begins with the optical pumping of both atoms into their required initial states of the entanglement generation scheme (atom A) and the storage scheme (atom B), respectively.

At node A, the atom is initialized in state $|F = 2, m_F = 0\rangle$. A π-polarized pump beam near-resonant with the atomic $F = 2 \leftrightarrow F' = 2$ transition of the D_1 line accumulates population in the desired state, since the $|2, 0\rangle \leftrightarrow |2, 0\rangle'$ transition is forbidden due to dipole selection rules, see e.g. [98]. As the $F = 2 \leftrightarrow F' = 2$ transition is not a closed transition, the atom can also decay into the state $F = 1$. For this reason, a π-polarized repumping laser near-resonant with the $F = 1 \leftrightarrow F' = 2$ transition on the on the D_2 line is applied to transfer population in $F = 1$ back into the pumping cycle.

Atom B is initialized in the $|F = 1, m_F = 0\rangle$ state by applying a π-polarized pump beam resonant with the Stark shifted atomic $F = 1 \leftrightarrow F' = 1$ transition on the D_2 line. Again, dipole selection rules forbid the $|1, 0\rangle \leftrightarrow |1, 0\rangle'$ transition and lead to accumulation of population in the desired state. As the atom can also decay into $F = 2$, a π-polarized repumping laser near-resonant with the $F = 2 \leftrightarrow F' = 1$ transition on the D_2 line, and on two-photon resonance with the cavity field is used to bring population lost to the $F = 2$ state back into the pumping cycle. For more details of the pumping scheme at node B, see [78].
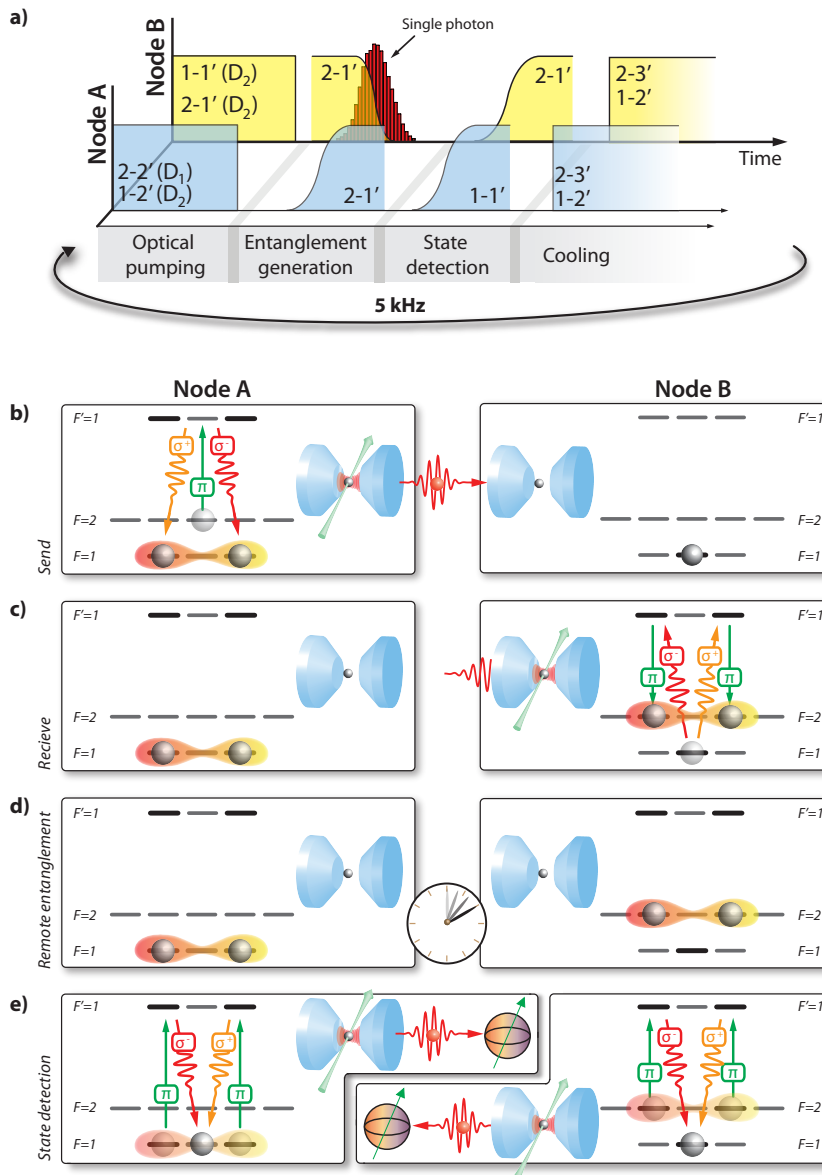
Figure 3.2.: Protocol of the remote entanglement experiment. a) Schematic of the experimental sequence: Shown are the laser pulses applied at each node and the transitions they address. The atoms are optically pumped into states $|2,0\rangle$ (node A) and $|1,0\rangle$ (node B), respectively. Then a photon entangled with the atom at node A is generated and coherently stored in the atom at node B. The entanglement is verified by mapping the atomic states onto the polarization of two photons and by performing state tomography on the photons. Before the sequence starts over, the atoms are cooled for approximately $150\,\mu s$. **b)-e)** Illustration of the single steps of the protocol: **b)** Atom-photon entanglement is created at node A. **c)** The photon is sent to and stored in the atom at node B. The photonic polarization state is mapped onto a superposition of Zeeman states of the atom, thereby creating remote entanglement between the two atoms. **d)** The atom-atom entangled state is preserved for up to $100\,\mu s$. **e)** The entanglement is verified by mapping the atomic states at each node onto the polarization state of a single photon which is subsequently detected.

Generation of atom-photon entanglement at node A

Following the optical pumping, a π-polarized control laser pulse coupling the $F = 2 \leftrightarrow F' = 1$ transition is applied to atom A and drives a vSTIRAP that generates a single photon in the cavity. Ideally, this results in the entangled $|\Psi^-\rangle$ Bell state of the atom and the photon given in Equation 2.14. The photon is coupled out of the cavity and sent to node B.

Photon storage at node B**. Remote atom-atom entanglement**

After optical pumping, the control laser at node B is switched on, also coupling the $F = 2 \leftrightarrow F' = 1$ transition. As soon as the photon from node A enters the cavity at node B, the control Rabi frequency Ω_C is decreased. During this step of the protocol, the polarization of the incoming photon is mapped onto a superposition of the Zeeman states $|2, \pm 1\rangle$ of atom B, and thus the atom-photon entanglement is converted into entanglement between the nodes, with the atoms in the maximally entangled $|\Psi^-\rangle$ Bell state:

$$\left|\Psi^-_{\mathrm{A}\otimes\mathrm{B}}\right\rangle = \frac{1}{\sqrt{2}}\left(|1, -1\rangle\,|2, +1\rangle - |1, +1\rangle\,|2, -1\rangle\right) \tag{3.1}$$

Read-out of the atomic states at nodes A **and** B

After a chosen time τ, the control fields at both nodes are ramped up again, mapping the atomic state of each atom onto the polarization of a single photon. The polarization states of these two photons are then measured and correlations between detection events in different polarization bases are analyzed to determine the entanglement fidelity or to reconstruct the density matrix of the entangled state.

3.1.4. Results

Efficiency

The success probability of generating entanglement of two single atoms at a distance is given by the product of the probabilities of the individual steps of the protocol – the efficiency η_A of generating a single photon at node A, the probability $T_{\mathrm{out}} = 0.9$ of this photon to leave the cavity through the outcoupling mirror, its successful transmission to the other cavity with probability T_{AB}, and the probability S to coherently store a photon impinging onto the cavity at node B:

$$P_{\mathrm{ent}} = \eta_{A1} T_{\mathrm{out}} T_{AB} S. \tag{3.2}$$

While the photon generation efficiency η_A and the transmission T_{AB} can easily be determined by independent measurements, the storage efficiency S is a figure that can only be inferred indirectly, because the method of using a reference photon as described in section 2.4 cannot be applied due to the fast-moving mirror. Instead, the storage efficiency is calculated by relating it to quantities that are experimentally accessible, as described in [78]. It is found to be 14 %.

Quantity	Value	Meaning
η_{A1}	0.4	Generation efficiency of atom-photon entanglement at node A
η_{A2}	0.03	Generation efficiency of a mapping photon at node A
η_B	0.6	Generation efficiency of the retrieved photon at node B
ϵ_A^D	0.28	Efficiency to detect an intra-cavity photon at node A, including fiber-coupling, transmission losses, and the quantum efficiency of the detectors
ϵ_B^D	0.32	Efficiency to detect an intra-cavity photon at node B, including fiber-coupling, transmission losses, and the quantum efficiency of the detectors
T_{out}	0.9	Outcoupling efficiency of the cavities into one single mode
T_{AB}	0.34	Transmission between nodes A and B, expressed as ratio of power measured before the fiber at node A and after the fiber at node B. Includes reflection off the fast-moving mirror
S	0.14	Efficiency of storing a single photon at node B

Table 3.1.: Efficiencies of the individual steps of the remote entanglement experiment.

Inserting the values given in Table 3.1 into Eq. (3.2), we find a success probability for the creation of remote entanglement of 2 %. The verification process for the entanglement, consisting of the production of one photon at each of the two nodes and their subsequent detection, has an efficiency of 0.16 %.

While the remote-entanglement protocol is repeated at a rate of $f = 5$ kHz, the actual rate of successful entanglement events is reduced by the condition that a single atom needs to be trapped at the center of each of the two cavities. The presented data were taken in the course of 10 hours of measurement. The combined duty cycle during that period, i.e. the fraction of time during which single atoms were present in both experiments simultaneously, was measured to be $D \approx 0.3$, resulting in a rate of 30 successful entanglement creations per second, or 3 detected events of a posteriori entanglement per minute. The main limiting factor for the detected entanglement event rate is the low efficiency of mapping the atomic state of atom A onto a photon, η_{A2}. As pointed out above, this rate is deliberately kept low to suppress off-resonant excitations to nearby hyperfine states.

Fidelity

As previously explained, several detrimental effects lead to the emission of uncorrelated photons during the read-out, and their evaluation cannot be avoided entirely. As this lowers the fidelity of the entangled state of the two photons compared to that of the two atoms before read-out, the fidelity we obtain constitutes a lower bound for the fidelity of the atom-atom entangled state.

The reconstructed density matrix of the entangled state, with the read-out performed 7 μs after the creation of atom-atom entanglement is shown in Fig. 3.3. We find a fidelity of $\mathcal{F} = (85 \pm 1.3)\,\%$ with the $|\Psi^-\rangle$ Bell state, which exceeds the classical limit of 50 % and clearly proves the existence of entanglement between the two atoms. The influence of dark counts of the detectors, which we assume to be randomly distributed, lies within the
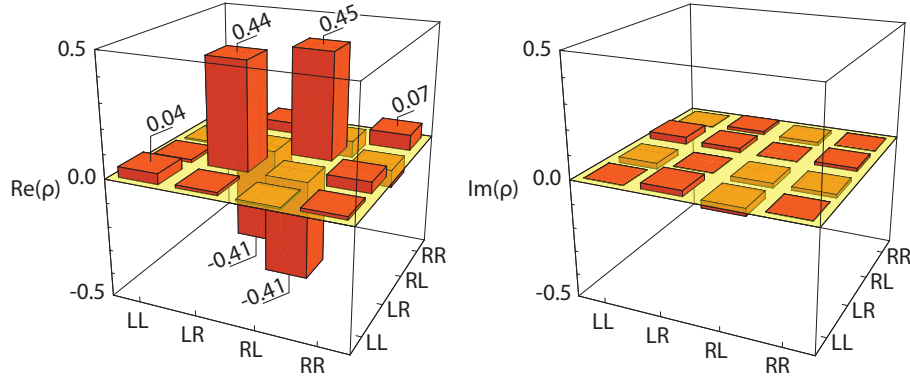
Figure 3.3.: Density matrix of the entangled state. Shown is the reconstructed density matrix, with the read-out of the atomic state performed 7 μs after the creation of atom-atom entanglement. The magnitudes of the elements of the imaginary part are ≤ 0.03. For an ideal $|\Psi^-\rangle$ Bell state, the inner diagonal (off-diagonal) elements of the real part have the value 0.5 (-0.5), respectively, indicating that the polarization of the detected photons is always orthogonal. The outer elements of the real part and the complete imaginary part are zero.

statistical error of the measured fidelity.

With further post-selection that I will elaborate on in the following section, fidelities as high as $(98.7 \pm 2.2)\,\%$ can be achieved.

The values given for the fidelity are the unbiased estimator and the statistical standard error. The likelihood function of $\mathcal{F}_{\Psi-}$ is non-Gaussian.

Post-selection and its effect on efficiency and fidelity

In order to find a more realistic value for the fidelity of the created atom-atom entangled state, we investigate the effect of post-selection of the acquired data. To this end, we apply our knowledge about detrimental effects when evaluating the data, without changing anything in the entanglement generation protocol itself.

The ideal Raman schemes from Figures 2.3 and 2.5 lead to the emission of single-photon wave packets with their polarization determined by the selection rules. The temporal envelope of the arrival time distribution of these photons is the sum of different wave packets whose temporal shape is determined by the a.c. Stark shift experienced by the atom at the moment of photon generation, but also by the actual transition undergone by the atom.

Several experimental imperfections cause deviations from the ideal Raman scheme: preparation of the initial state, misaligned polarization of the control laser, and off-resonant excitations. As described in chapter 2, these imperfections not only affect polarization correlations, they also influence the temporal envelope of the wave packet of the emitted photons. Imperfections are generally correlated with delayed photon emission with respect to the ideal Raman scheme. Therefore, the contribution of the non-ideal processes to the measured fidelity can be minimized if only those photon detection events are evaluated that occur early in the temporal wave packet of the photon.

The efficiencies and fidelity stated above were obtained by analyzing all read-out photons from node A and those photons from node B arriving within a 1 µs time interval centered around the maximum of the photon wave packet, as depicted in Fig. 3.4 **a)**.

Considering for instance only the first 40 % of the ensemble of detected photons from node A and the initial 20 % of the ensemble of photons from node B, the fidelity is increased to (98.7 ± 2.2) %. Obviously, post-selection on the arrival-times of the analyzed photons enhances the fidelity, while the reduced number of events contributing to the evaluation leads to a decrease in efficiency, as is shown in Fig. 3.4 **b)** and **c)**.

Another way of suppressing imperfections correlated with late photon emission is to tailor the read-out process directly. This is achieved by keeping the control laser Rabi frequency Ω_C of the read-out pulse low and applying it for a short time only. In doing so, the read-out photon can be made to resemble the post-selected subset. This weak read-out was used at node A, thereby optimizing for high fidelities at the expense of the efficiency of the verification process.

## Lifetime of the entangled state

The lifetime of the entangled state of the two atoms is limited by decoherence, which is dominated by dephasing caused by uncorrelated magnetic field fluctuations on the order of 1 mG at the two individual nodes, and position-dependent differential a.c. Stark shifts induced by the dipole trap fields.

Depending on their orientation relative to the quantization axis of our systems, magnetic fields have different effects on the Zeeman states carrying the information of the entangled state. In the presence of a magnetic field $B_\parallel$ parallel to the quantization axis, the atomic states $|2, \pm 1\rangle$ ($|1, \pm 1\rangle$) experience a Zeeman shift of $\Delta E = \mu_B g_F m_F B_\parallel$, with Bohr's magneton $\mu_B = e\hbar/2m_e$, and the Landé factor $g_{F=2} = \frac{1}{2}$ ($g_{F=1} = -\frac{1}{2}$). Therefore, they undergo a different time evolution, leading to the accumulation of a relative phase between the states with $m_F = +1$ and -1.

Magnetic fields $B_\perp$ perpendicular to the quantization axis also lead to an energy splitting, but the Larmor precession around the axis of the magnetic field results in a mixing of the Zeeman states defined with respect to the quantization axis.

Applying a small magnetic guiding field B_0 along the quantization axis of each node can significantly reduce the dephasing due to local magnetic field fluctuations. While such a field leads to a controlled phase evolution between the Zeeman substates, the influence of transversal fluctuations $B_\perp$ is suppressed by a factor of $B_\perp/2B_0$. If guiding fields of equal strength are applied to both nodes, the atoms remain in the entangled $|\Psi^-\rangle$ Bell state all the time, since the relative phase between the atomic qubits remains unchanged. We have previously demonstrated that guiding fields of approximately 30 mG improve the coherence times of the individual systems to almost 200 µs [83, 101].

For the coupled systems, with guiding fields applied in both laboratories, we observe highly non-classical correlations between the two atoms for 100 µs. The fidelity with the $|\Psi^-\rangle$ Bell state measured 100 µs after the entanglement creation is (56 ± 3)% and thus two standard deviations above the classical limit of 50 %. The observed lifetime of the entangled state
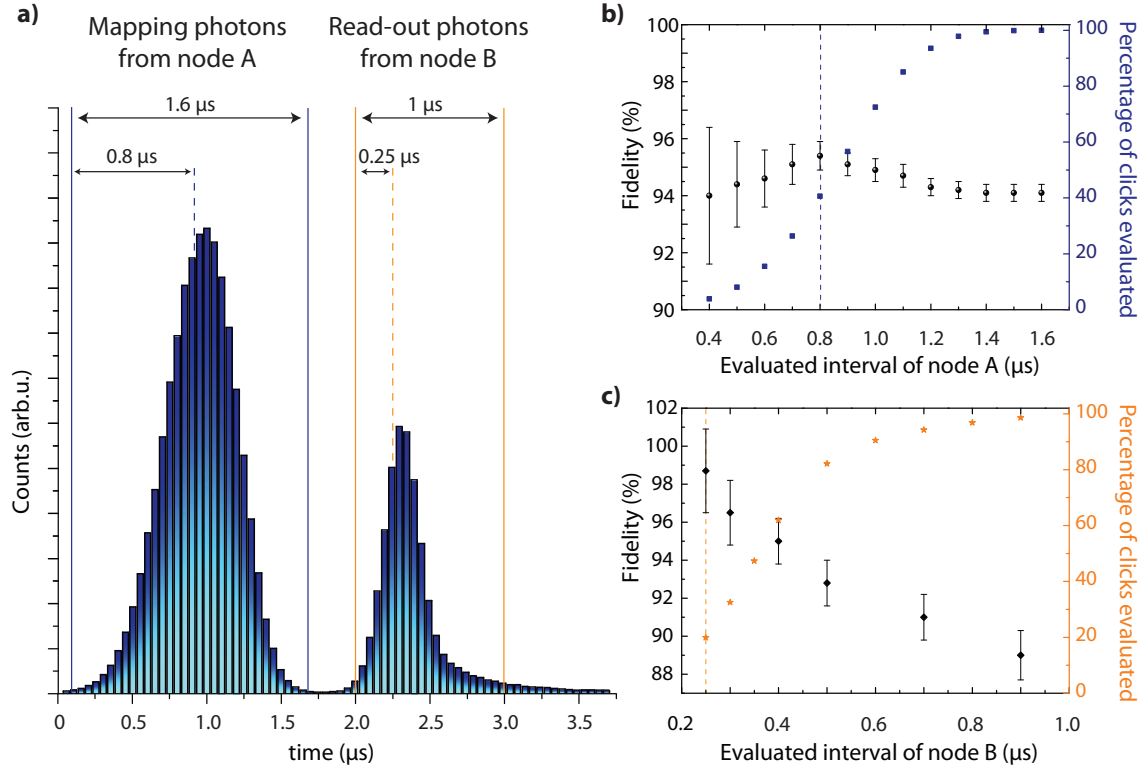
Figure 3.4.: Post-selection on the arrival times of the detected photons. a) Integrated arrival time histogram showing the envelopes of the mapping photons from node *A* and the retrieved photons from node *B*. Solid lines indicate the full evaluation intervals, dashed lines intervals selecting photons that arrived early. **b)** Local measurement of photon-photon entanglement at node *A* without storage in node *B*: Plotted is the measured fidelity with the $|\Psi^-\rangle$ Bell state (black circles), and the efficiency (blue squares) as a function of the length of the evaluation interval of the mapping photon. Post-selection on early arrival times improves the fidelity by $\approx 1.5\,\%$. A similar effect of post-selection on the arrival time of entangling photon is not observed. **c)** Remote entanglement measurement: The entangled state of the two atoms is mapped onto photon-photon entanglement. The plot shows the measured fidelity with the $|\Psi^-\rangle$ Bell state (black circles) and the efficiency (orange stars) of the evaluation as a function of the length of the evaluation interval of the read-out photon from node *B*. For this plot, the evaluation interval of the mapping photon was $0.8\,\mu\text{s}$ long. The increase in fidelity to a value higher than in the independent local measurement from **b)** could have different reasons: While we did not observe an effect of post-selection on the entangling photon, it might still be the case that photons resulting from unwanted transitions have properties that make them less likely to be stored, leading to them being filtered out. Another reason could be that, in the local measurement, the atomic state is projected immediately by the detection of the entangling photon and is subject to decoherence and dephasing until the atomic state is mapped $7\,\mu\text{s}$ later. The entangled state of the two distant atoms is also read out after $7\,\mu\text{s}$, but common noise in both atom-cavity systems during that time, however unlikely, might lead to a higher fidelity. All quoted errors are statistical.
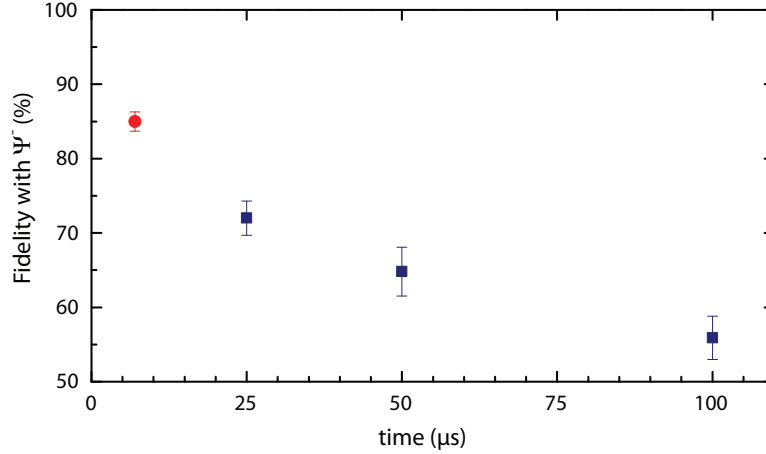
Figure 3.5.: Lifetime of the entangled state of the two single atoms. Plotted is the measured fidelity of the entangled state as a function of time between entanglement creation and readout. The data point at 7 µs (red circle) corresponds to the density matrix shown in Fig. 3.3 and was obtained from measurements at zero magnetic field. For the measurements of the other data points (blue squares) magnetic guiding fields of 30 mG along the cavity axis were applied at both nodes. The offset of 50 % corresponds to the classical limit.

exceeds the entanglement creation time (1 µs for creation, transmission and storage of an entangling photon) by two orders of magnitude.

Measurements of the fidelity for different storage times are plotted in Fig. 3.5. Note that it is crucial for such measurements that identical guiding fields are applied in both laboratories. A difference in the applied fields will lead to accumulation of a relative phase between the constituents of the entangled state resulting in a rotation of the entangled state. Such a rotation can also be introduced on purpose, as I will show in the next section.
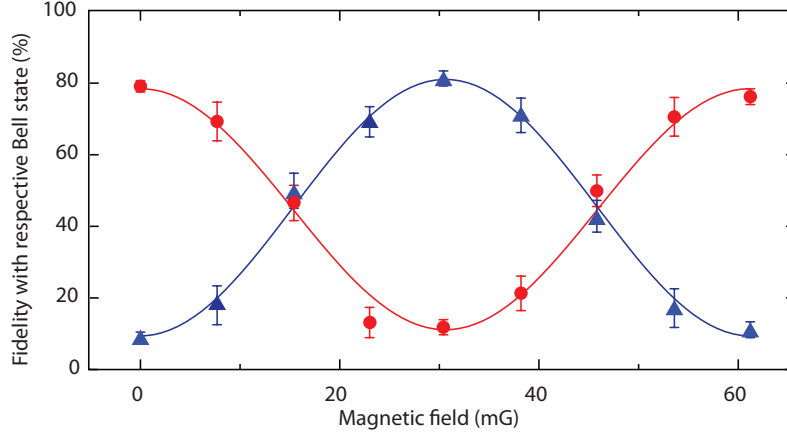
Controlled rotation of the entangled state

Since nodes A and B are in separate physical locations, they are independently addressable for local qubit control.

When the atoms at the two nodes are entangled, a unitary operation applied locally at just one of the nodes changes the non-local state of both nodes without destroying the entanglement. Using a single initial entangled state as a resource, local qubit control therefore allows arbitrary maximally entangled two-qubit states to be created. We demonstrate this capability by creating the $|\Psi^+\rangle$ Bell state.

The two atoms are initially prepared in the entangled $|\Psi^-\rangle$ Bell state as described before. Applying a magnetic guiding field along the quantization axis of one of the cavities (node B) leads to the accumulation of a phase between the Zeeman substates the qubit is encoded in, $|F = 2, m_F \pm 1\rangle$, and causes a state rotation at twice the Larmor frequency, $\omega_L = B_0\mu_B/\hbar g_F$:

$$\left|\Psi_{\mathrm{AB}}^-\right\rangle = \frac{1}{\sqrt{2}}\left(|1,-1\rangle\,|2,+1\rangle - e^{2i\omega_L t}\,|1,+1\rangle\,|2,-1\rangle\right). \tag{3.3}$$

Figure 3.6.: Controlled rotation of the entangled state. The non-local quantum state of the entangled nodes is changed by locally applying a magnetic field to the atom B, while atom A is held at zero magnetic field. For the fixed hold-time of $12.5\,\mu s$, the fidelity with the $|\Psi^-\rangle$ and $|\Psi^+\rangle$ Bell state (red and blue data, respectively) is plotted as a function of the applied magnetic field. The solid lines are sine and cosine fits to guide the eye. The error bars indicate the statistical standard error.

To observe this rotation, one can either keep the guiding field B_0 at a fixed value and vary the time τ between entanglement creation and read-out of the atomic states, or vice-versa. In Fig. 3.6, the fidelity of the created state with the $|\Psi^-\rangle$ and $|\Psi^+\rangle$ Bell state is plotted as a function of the magnetic field applied to node B. The time between entanglement creation and read-out is fixed at $12.5\,\mu s$.

We start by preparing the two atoms in the $|\Psi^-\rangle$ Bell state. After the hold time of $12.5\,\mu s$ with no magnetic fields applied at either of the nodes, we measure a fidelity of $\mathcal{F}_{\Psi^-} = (79 \pm 1.6)\,\%$. Using a magnetic field of $30\,mG$ at node B, the $|\Psi^-\rangle$ Bell state is rotated into a $|\Psi^+\rangle$ state of comparable fidelity $\mathcal{F}_{\Psi^+} = (81 \pm 2)\,\%$. The original $|\Psi^-\rangle$ state is recovered at a magnetic field of $60\,mG$ and after a spin rotation of 2π with a fidelity of $(76 \pm 2)\,\%$. The reduced fidelity here is a result of the non-negligible Larmor precession during the entanglement creation and read-out process, the duration of both of which is on the order of $1\,\mu s$.

3.2. Remote entanglement between a single atom and a Bose-Einstein condensate

Future realizations of quantum networks will not necessarily rely on identical nodes. In fact, it is more likely that a network will comprise different elements or components not all of which have full functionality. Instead, one can for instance think of sources of single or possibly entangled photons with no or limited quantum memory capacity, which are combined with other systems that have excellent memory properties but cannot generate single photons. Those quantum memories might even offer the possibility of gate operations on one or several stored qubits [108].

Eventually, the result could be a hybrid architecture that brings together single ions and atoms, ensembles, quantum dots and NV centers, linear optical circuits, microwave technologies and so forth. Ideally, a future quantum network will benefit from the merits of the different approaches, while at the same time compensating for their individual weaknesses. The challenge in realizing such a network lies in meeting the requirements of these various components regarding e.g. the transition frequencies and temporal envelope of the photons exchanged, which can significantly differ for each component.

This section explores remote entanglement in a hybrid, albeit atom based realization. Entanglement is created between two conceptually very different systems: a single atom in a cavity on one hand, and about a million atoms in a Bose-Einstein condensate (BEC) on the other.

I will only give a brief summary of the results of this experiment. A more detailed discussion can be found in the dissertation of my colleague Matthias Lettner [84]. The content of this section has been partially published in

Remote Entanglement between a Single Atom and a Bose-Einstein Condensate.
M. Lettner, M. Mücke, S. Riedl, C. Vo, C. Hahn, S. Baur, J. Bochmann, S. Ritter, S. Dürr, and G. Rempe, *Physical Review Letters* **106**, 210503 (2011)

3.2.1. Experimental protocol

The experimental protocol for the creation of entanglement between a single atom and a BEC is almost identical with the one for the creation of entanglement between the two single atoms, described in Sec. 3.1.3.

The first step is the creation of atom-photon entanglement, see Fig. 3.7 **a)**. The generated photon is transferred to and coherently stored in the BEC, again with a storage process based on the control of a coherent dark state, exploiting to the phenomenon of electromagnetically induced transparency [109, 110]. When a single photon is stored, it is converted into a single magnon, as shown in Fig. 3.7, **b)**. This is a quasiparticle of a collective spin-wave excitation on the BEC, which can be expressed by

$$|2,\pm 1\rangle_{\mathrm{BEC}} = \frac{1}{\sqrt{N}} \sum_{i=1}^{N} |2,\pm 1\rangle \, |\chi_2\rangle_i \prod_{j=1,j\neq i}^{N} |1,0\rangle \, |\chi_1\rangle_j \,, \tag{3.4}$$

where $|\ldots\rangle_i$ denotes the state of the ith atom in the BEC, χ_1 and χ_2 are spatial wave functions, and N is the number of atoms in the BEC. Correspondingly , the entangled state between the single atom and the BEC is

$$\left|\Psi^-\right\rangle_{\mathrm{atom}\otimes\mathrm{BEC}} = \frac{1}{\sqrt{2}} \left(|1,-1\rangle_{\mathrm{atom}} |2,+1\rangle_{\mathrm{BEC}} - |1,+1\rangle_{\mathrm{atom}} |2,-1\rangle_{\mathrm{BEC}} \right). \tag{3.5}$$

All atoms in the BEC participate in the collective excitation, so the single atom is entangled with an enormous number of atoms [111].

To verify the entanglement, the matter-matter entangled state is converted into the entangled state of two photons known from Eq. (2.15), which is subsequently detected.
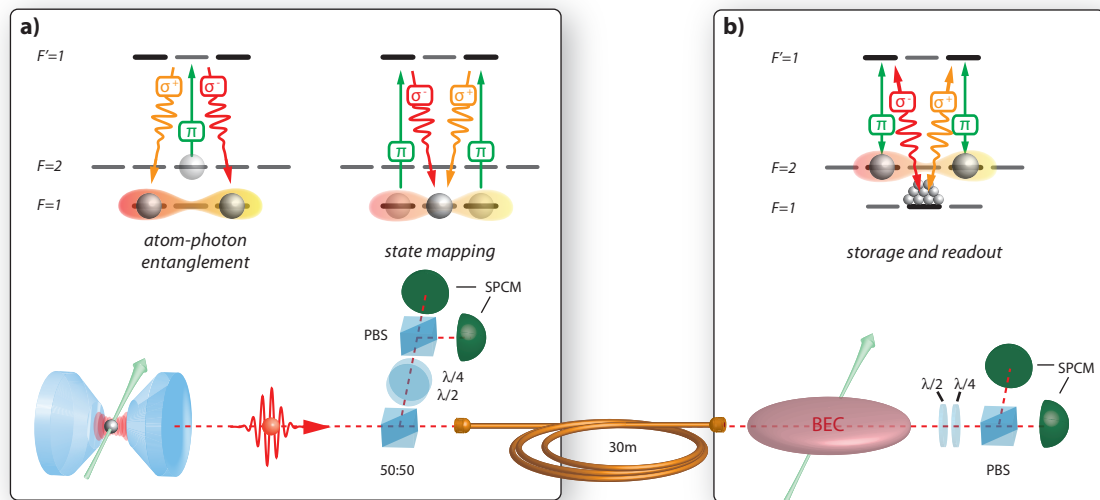
Figure 3.7.: Remote entanglement between a single atom and a BEC – protocol and implementation. a) Entanglement between the single atom and a single photon is created. The photon passes a non-polarizing 50:50 beamsplitter and is coupled into an optical fiber connecting the atom-cavity experiment with the BEC experiment. **b)** By coherently storing the photon in the BEC, entanglement between the single atom and the BEC is established. After a variable hold time, the atomic qubits in both laboratories are mapped onto the polarization state of single photons which are measured in independent detection setups formed by $\lambda/2$ and $\lambda/4$ waveplates allowing for the detection in different polarization bases, a polarizing beam splitter (PBS), and single photon counting modules (SPCM).

3.2.2. Experimental implementation

Even though both the atom-cavity experiment and the BEC experiment are based on ^{87}Rb, they are fundamentally different. Finding optimal working parameters poses a much greater challenge than in the case of the two quasi-identical atom-cavity experiments described in Sec. 3.1.

The critical parameter is the frequency of the photon to be exchanged between the two systems. Its choice affects the photon generation efficiency of the atom-cavity system and the write-read efficiency of the BEC experiment alike. Optimizing the performance of each system for stand-alone operation produces quite different values for the optimal frequency, both on a coarse scale of D_1 versus D_2 line and on a fine scale of tens of MHz. The compromise made in order to couple the two setups required each experiment to work outside its optimal set of parameters.

Off-resonant photoassociation in the BEC experiment causes the atom number to decay 50 times faster when working on the D_2 line compared to the D_1 line. However, the photon generation efficiency of the atom-cavity system is significantly smaller on the D_1 line, as described in Sec. 2.3. In addition, the optical dipole trap which holds the single atom shifts the atomic resonance by 130 MHz. The final compromise to work on the D_1 line at a blue detuning of 70 MHz relative to the free-space resonance optimizes the overall efficiency of the entanglement protocol. It is a tradeoff between the reduced write-read

efficiency of the BEC and the reduced photon production efficiency of the atom-cavity system. The resulting efficiencies are $\eta_{\mathrm{BEC}} = 16\%$ and $\eta_{\mathrm{atom}} = 14\%$.

The other big difference of this experiment compared to the coupling of the two atom-cavity systems is the very different duty cycles, the fraction of time where data taking is possible. Creating a BEC with a million atoms takes about 18 s. Then some 10^4 write-read cycles can be performed before the number of atoms N in the condensate and with it the efficiency η_{BEC} has dropped so much that it becomes necessary to stop the sequence and start preparing a new BEC. This results in a duty cycle of the BEC experiment alone of only 10 %.

Loading a single atom on the other hand takes 1.4 s, which includes loading the MOT, transferring the atom to the standing-wave trap and evaluating a camera image to verify the presence of a single atom. Since the loading process is probabilistic, the effective loading time for a single atom is longer. The success probability of loading a single atom per run of the BEC was measured to be 72 % [83], further diminishing the duty cycle.

Once a BEC is prepared and a single atom is present, the entanglement protocol is started and repeated at a 10 kHz rate until the atom is lost or a new BEC needs to be prepared. Like in the atom-atom entanglement experiment, both systems are synchronized by a master clock, and light from a frequency comb is used as a reference.

Photons generated with the atom-cavity system are sent onto a 50:50 beamsplitter which directs them either to a detection setup or, via a 30 m long optical fiber, to the BEC experiment. After storage and retrieval there, they are directed to a second detection setup, see Fig. 3.7. Unwanted polarization rotations along the path of the photons are compensated for and it is ensured that the input polarization of one detection setup matches that of the other.

3.2.3. Results

The entanglement between the single atom and the BEC is verified a posteriori by the analysis of polarization correlations between the photons retrieved from the atom and the BEC.

Figure 3.8 shows the reconstructed density matrix of the two-photon state for a read-out and mapping 1 µs after the creation of remote entanglement. The measured fidelity with the expected $|\Psi^-\rangle$ Bell state is $\mathcal{F} = (95.0 \pm 3.4)\%$. Comparison with the fidelity of entangled photons generated from the atom-cavity system without storage of one of the photons in the BEC, $\mathcal{F} = (94.1 \pm 1.5)\%$, shows that the entanglement experiences no significant degradation by the conversions in the storage and retrieval process. In that respect, the Bose-Einstein condensate is an excellent quantum memory.

We also characterized the lifetime of the entangled state and investigated the effect of the individual dephasing of the two subsystems. In Fig. 3.9, the measured fidelity $\mathcal{F}_{\Psi^-}$ is plotted as a function of time. For the green data points, the atomic states in both systems are projected onto single photons at equal times $t_{\mathrm{atom}} = t_{\mathrm{BEC}}$ after the creation of the entangled state. After a lifetime of 100 µs, the fidelity is still $\mathcal{F} = (68 \pm 7)\%$ and therefore exceeds the classical limit of 50 % by more than 2 standard deviations. For the pink and
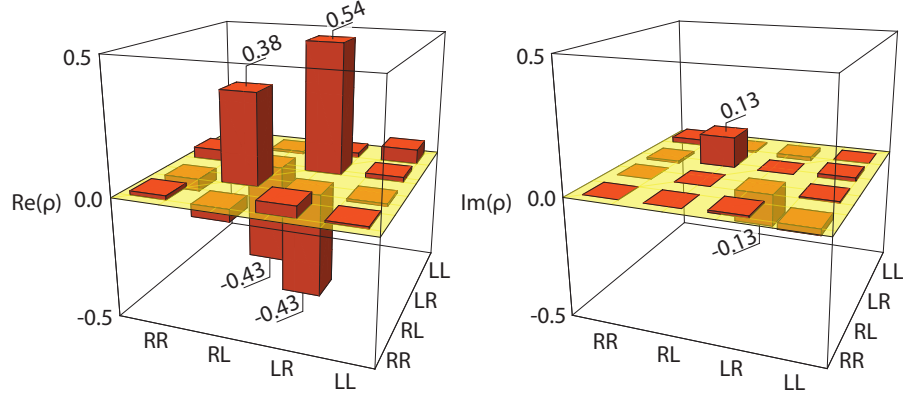
Figure 3.8.: Density matrix of the entangled state of the single atom and the BEC.
Shown are the real and imaginary part of the reconstructed density matrix, with the state mapping
and read-out performed 1 μs after the entanglement creation. The statistical error of the matrix
elements is 0.04. The fidelity with the expected $|\Psi^-\rangle$ Bell state is $\mathcal{F} = (95.0 \pm 3.4)\,\%$.
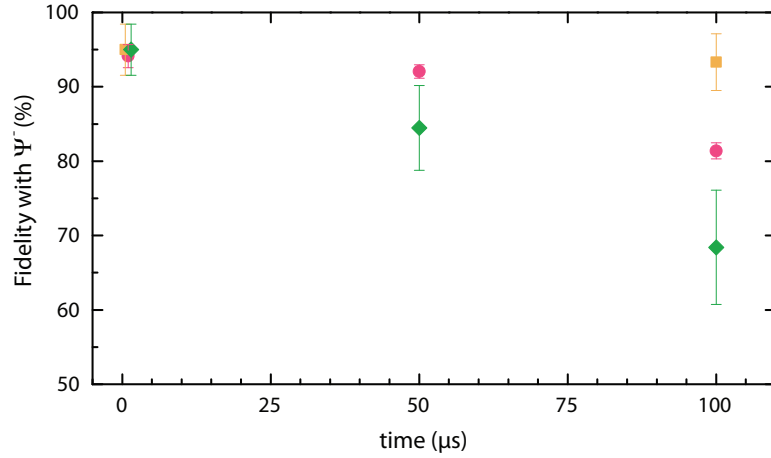
Figure 3.9.: Lifetime of the entangled state of the single atom and the BEC. Green
diamonds represent the measured fidelity of the entangled state for different read-out times $t_{\text{atom}} = t_{\text{BEC}}$ after the entanglement was established. Pink circles are the fidelity of the entangled state
of the two photons generated from the atom-cavity system without storage in the BEC. For the
orange squares, the state of the atom was mapped on a photon after $t_{\text{atom}} = 1\,\mu$s and the retrieval
time t_{BEC} was varied. For better visibility, the data-points at 1 μs are offset by 500 ns. The offset
of 50 % corresponds to the classical limit.

orange data points, only one of the systems experiences dephasing, while the atomic state of the other system is projected immediately.

As discussed earlier, see Sec. 3.1.4, the main reason for dephasing is local fluctuations of the magnetic field. For the lifetime measurements depicted in Fig. 3.9, magnetic guiding fields of $40\,\mathrm{mG}$ in the atom-cavity system and $100\,\mathrm{mG}$ in the BEC experiment were applied along the respective quantization axes to suppress the influence of transversal magnetic field fluctuations. From Fig. 3.9 it is obvious that the BEC is better isolated from the disturbing influences of its surroundings than the single atom in the cavity. The reason for this is twofold: The stronger guiding field in the BEC experiment suppresses fluctuations of the magnetic field more strongly than in the atom-cavity system. There, a much stonger guiding field would have been impractial, since significant Larmor precession during the generation of a photon leads to a decrease in fidelity. In addition, in the BEC experiment some periodic fluctuations are compensated by means of a feed forward to the guiding field.

The main limitation of the presented experiments is the very low probability of detecting two-photon correlations, which was typically 10^{-6} per experimental run, or one correlation every seven minutes in actual measurement time. To overcome this limitation is certainly challenging [83, 84]. Nevertheless, the possible applications of hybrid approaches in quantum information processing, in particular the possibility to employ different constituents of hybrid quantum systems in order to realize distinct functionalities, promise that further investigation will be rewarding.

4. Conclusion and outlook

In this thesis, I have presented the entanglement of two single atoms at a distance of 21 m, realized by the coherent exchange of a single photon. This new scheme and the enhanced light-matter coupling achieved by placing the single atoms in optical resonators permit unprecedented values for the efficiency of the entanglement creation and the fidelity of the entangled state. Compared to all other remote entanglement experiments with single particles in free space so far, which relied on entanglement swapping [24, 67], we demonstrate an increase of five orders of magnitude in efficiency and three orders of magnitude in success rate.

In the following, I propose potential improvements of our experimental setup, before I discuss the prospects of single emitters in cavities for future quantum networking applications. The main limitation to the efficiency of our entanglement protocol is our moderate atom-cavity coupling g, which affects the maximum achievable single-photon generation and storage efficiency alike. The most straightforward way of enhancing this coupling in the current setup is to confine the atom more strongly with respect to the cavity mode, thereby minimizing variations in g [106]. Photon generation and storage efficiencies approaching unity may be reached by decreasing the mode volume of the cavity, for instance by using fiber-based optical cavities [112, 113]. The efficiency of the storage process, and, consequently, of the generation of remote entanglement, may be increased by improved impedance matching [114]. To this end, more elaborate shaping of the temporal envelope of the control laser can further minimize the amount of light reflected off the cavity. Dismissing the virtues of single-particle network nodes regarding the efficient generation of atom-photon entanglement, one could instead opt for an atomic ensemble collectively coupled to the cavity mode, as this might dramatically increase the storage efficiency. In the current setup, however, the benefit of collective strong coupling is outweighed by another collective effect, namely, dephasing of the spin wave of the stored excitation, which causes a time-dependence of the storage efficiency so strong that it is rendered impractical to work with. This limitation should be overcome by better confinement and/or lower temperatures of the ensemble.

The efficiency of the entanglement verification is additionally limited by the weak read-out of the atom at node A. In the current implementation, the efficiency of the state mapping is deliberately kept low to suppress off-resonant excitations to nearby hyperfine states. This problem is specific to a qubit encoded in the $F = 1$ manifold and could be avoided by a local transfer of the qubit to the $F = 2$ manifold, using optical Raman or microwave pulses [106, 108]. Such a transfer could improve the efficiency of the verification step by a factor of 20, if we assume unity transfer efficiency and our maximum photon generation efficiency of 60% (cf. chapter 2).

In its current implementation, our entanglement scheme does not include a herald that

signals that an attempt to create entanglement was successful. A possible implementation could rely on cavity-assisted detection of the atomic hyperfine state [115, 116, 117]. Storing a photon changes the hyperfine state of the atom, so one would simply test whether any population is left in the initial state, either by detecting fluorescence or by monitoring the cavity transmission. Due to the large ground state splitting of ^{87}Rb, a qubit encoded in $F = 2$ should remain undisturbed when $F = 1$ is probed. Fluorescence detection relies on photon generation on the closed $F = 1 \leftrightarrow F' = 0$ transition. It is challenging, since one has to ensure that population remaining in $F = 1$ is detected with high fidelity before off-resonant excitation to another excited state leads to decay and therefore loss of the atom to $F = 2$, which in our current setup is expected to occur typically after only a few scattered photons [78]. An alternative scheme relies on the fact that the cavity transmission is largely suppressed for a strongly coupled atom. This can be used to probe the internal state of the atom. However, only weak probing is allowed since excitation of the system needs to be avoided. At the same time it is necessary to obtain a high-fidelity signal within the coherence time of the qubit. While the implementation of a herald is challenging with our current setup, it is not entirely out of reach even with current cavity technology [108, 117], where a smaller cavity mode volume or better confinement of the atoms with respect to the cavity mode lead to stronger atom-cavity coupling and in turn to a higher Purcell factor.

Our cavity-based approach to quantum networking and the resulting success probabilities constitute an important step towards the realization of large-scale quantum networks with arbitrary topologies. Simply using classical optics, our elementary network can easily be extended to more complex geometries. In addition, the use of cavities paves the way towards hybrid architectures in such networks, since, at least to some extent, problems arising from differing transition frequencies of the various systems under consideration can be overcome. In particular, it opens up new perspectives for solid-state-based approaches to quantum networking, such as quantum dots and color centers in diamond [118, 119, 120, 121].

The quasi-deterministic scheme for remote entanglement generation presented in this thesis, together with the possibility of entanglement swapping [24, 66, 67], and the ability to perform quantum teleportation, which we have demonstrated in [100], pave the way for long distance quantum communication. By employing single-atom registers [122], the number of qubits per node may be increased. After creating remote atom-atom entanglement following the protocol described in this thesis, the registers at different nodes could be shifted to successively produce many sets of entangled atoms. Those could then be used, for instance, for nested entanglement purification. In combination with the long storage times achievable with single atoms and the potential for heralding, this possibility represents a realistic avenue towards quantum communication over arbitrary distances by means of a quantum repeater protocol [44]. Moreover, our experiments bring quantum communication between atoms into a regime where the time needed for a successful entanglement build-up attempt (0.2 s at a repetition rate of 5 kHz) is shorter than coherence times observed in single atoms [123]. This is essential for any quantum repeater architecture, where coherence needs to be maintained while a repeat-until-success scheme is used to establish long-distance entanglement.

A. Effect of thermal motion on the efficiency of storage in an atomic ensemble

To understand the difference between storage in a single atom and storage in an ensemble, it is necessary to review the individual steps of the storage protocol: storage, retrieval, and especially the dark time in between. A simplified theoretical model for an atomic ensemble in free space is derived to estimate the effect of thermal motion on the efficiency of the memory. For the sake of convenience, the following considerations are restricted to the atomic ground states $|F = 1\rangle$ and $|2\rangle$ involved in the storage protocol. The conclusions apply to the full scheme nevertheless.

Storage

Initially, all N atoms of the ensemble are prepared in the internal state $|1\rangle$. The state of the ensemble can be written as

$$|1_1 \ldots 1_N\rangle = \prod_j u_j(\boldsymbol{r}_j) |1_j\rangle \qquad (A.1)$$

where $u_j(\boldsymbol{r}_j) = \exp(i\boldsymbol{k}_j\boldsymbol{r}_j)/\sqrt{V_{qu}}$ is the motional wave function of the j-th atom with initial momentum $\boldsymbol{k}_j$, and V_{qu} is the quantization volume.

The process of storing a single photon brings the population into a coherent superposition expressed by the Dicke state

$$|D(t = 0)\rangle = \frac{1}{\sqrt{N}} \sum_j \exp(i\boldsymbol{k}_{rec}\boldsymbol{r}_j) |1_1 \ldots 2_j \ldots 1_N\rangle. \qquad (A.2)$$

During the transfer, the j-th atom is transferred from state $|1\rangle$ into state $|2\rangle$ and picks up a differential recoil, resulting in the position-dependent phase factor $\exp(i\boldsymbol{k}_{rec}\boldsymbol{r}_j)$. Above, the following abbreviation was used:

$$|1_1 \ldots 2_j \ldots 1_N\rangle = u_j(\boldsymbol{r}_j) |2_j\rangle \prod_{l \neq j} u_l(\boldsymbol{r}_l) |1_l\rangle. \qquad (A.3)$$

Note that $\langle 1_1 \ldots 2_j \ldots 1_N | 1_1 \ldots 2_l \ldots 1_N\rangle = \delta_{jl}$.

Dark time

During the time between storage and read-out, each term in the sum in $|D(t)\rangle$ picks up a phase $\exp(-iEt/\hbar)$ with energy E. If the zero of the energy is chosen in such a way that

the internal state with exactly one excitation has zero energy, only kinetic energy remains. The evolved state is

$$
\begin{aligned}
|D(t)\rangle &= \frac{1}{\sqrt{N}} \sum_j \exp(i\boldsymbol{k}_{rec}\boldsymbol{r}_j) |1_1 \ldots 2_j \ldots 1_N\rangle \exp\left(-it\frac{\hbar}{2m}\left((\boldsymbol{k}_{rec} + \boldsymbol{k}_j)^2 + \sum_{l \neq j} k_l^2\right)\right) \\
&= \exp\left(-it\frac{\hbar}{2m}(k_{rec}^2 + \sum_l k_l^2)\right) \frac{1}{\sqrt{N}} \sum_j \exp\left(i\boldsymbol{k}_{rec}(\boldsymbol{r}_j - \boldsymbol{v}_j t)\right) |1_1 \ldots 2_j \ldots 1_N\rangle
\end{aligned}
\tag{A.4}
$$

with $\boldsymbol{v}_j = \hbar\boldsymbol{k}_j/m$. This is still a Dicke state but with a different global phase and different relative phases between the terms.

Retrieval

The laser light of the read-out pulse couples only to the state $|D(0)\rangle$, and ideally the retrieval process converts amplitude in $|D(0)\rangle$ completely into a retrieved state $|\psi_{ret}\rangle$. This retrieved state has no $|F = 2\rangle$ contribution, so $\langle\psi_{ret}|D(t)\rangle = 0$ for all t. We choose an orthonormal basis $(|v_1\rangle, |v_2\rangle, \ldots)$ with $|v_1\rangle = |\psi_{ret}\rangle$ and $|v_2\rangle = |D(0)\rangle$. The time evolution operator of the read-out ideally has the form

$$
U_{ret} = i\left(|\psi_{ret}\rangle \langle D(0)| + \text{H.c.}\right) + \sum_{j \notin 1,2} |v_j\rangle \langle v_j|
\tag{A.5}
$$

The state after retrieval is therefore

$$
|\psi_{out}\rangle = U_{ret} |D(t)\rangle = i |\psi_{ret}\rangle \langle D(0)|D(t)\rangle + \sum_{j \notin 1,2} |v_j\rangle \langle v_j|D(t)\rangle
\tag{A.6}
$$

with $\langle\psi_{ret}|D(t)\rangle = 0$ from above.

Let $\hat{N}_{ret}$ denote the operator for the number of retrieved photons. Then $\hat{N}_{ret}$ is diagonal in the basis $(|v_1\rangle, |v_2\rangle, \ldots)$ with eigenvalues $\hat{N}_{ret} |v_j\rangle = \delta_{j1} |v_j\rangle$ since all states other than the retrieved state do not contribute retrieved photons. Hence $\hat{N}_{ret} = |\psi_{ret}\rangle \langle\psi_{ret}|$. The expectation value of the retrieved photon number is therefore

$$
\langle\psi_{out}| \hat{N}_{ret} |\psi_{out}\rangle = |\langle\psi_{ret}|\psi_{out}\rangle|^2 = |\langle D(0)|D(t)\rangle|^2.
\tag{A.7}
$$

As we assumed exactly one incoming photon $N_{in} = 1$, the write-read efficiency is $\eta_{wr} = \langle\hat{N}_{ret}\rangle$. Therefore
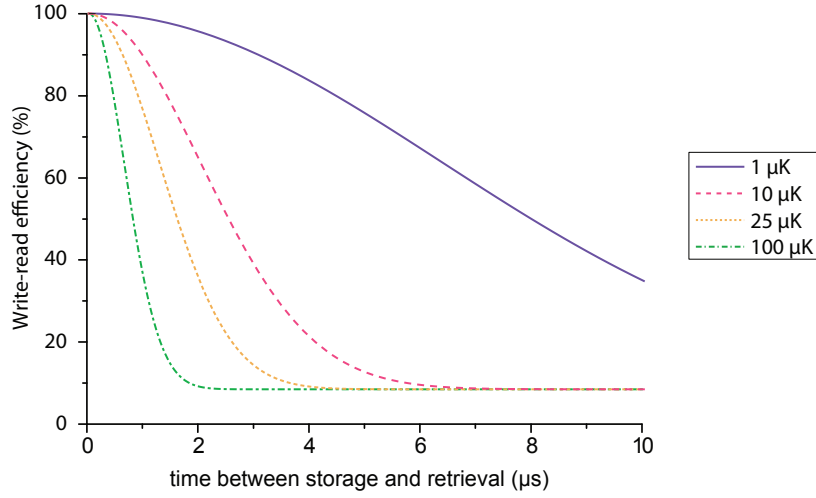
$$
\eta_{wr} = \eta_0 \left| \langle D(0)|D(t)\rangle \right|^2,
\tag{A.8}
$$

where η_0 accounts for finite efficiency at $t = 0$. The overlap of these states is

$$
\langle D(0)|D(t)\rangle = \exp\left(-it\frac{\hbar}{2m}(k_{rec}^2 + \sum_l k_l^2)\right) \frac{1}{N} \sum_j \exp(-i\boldsymbol{v}_j t\boldsymbol{k}_{rec}),
\tag{A.9}
$$

and, using $\boldsymbol{v}_{rec} = \hbar\boldsymbol{k}_{rec}/m$, its modulus squared is

$$
\eta_{wr} = \eta_0 \left| \frac{1}{N} \sum_j \exp(-i\boldsymbol{v}_{rec} t\boldsymbol{k}_j) \right|^2 = \frac{\eta_0}{N^2}\left(N + \sum_{j,l,j\neq l} \exp\left(i\boldsymbol{v}_{rec} t(\boldsymbol{k}_j - \boldsymbol{k}_l)\right)\right).
\tag{A.10}
$$

Figure A.1.: Effect of thermal motion on the write-read efficiency: Theoretical prediction of the time dependence for $N = 12$ atoms and different temperatures.

Effects of thermal averaging

We consider a thermal Boltzmann distribution, so the wave vectors of different atoms are uncorrelated and the single-particle distribution is given by

$$p(\boldsymbol{k}_j) = \frac{1}{(2\pi)^{1/2}\sigma_{k_z}} \exp\left(-\frac{k_j^2}{2\sigma_{k_z}^2}\right) \tag{A.11}$$

with the one-dimensional rms-width $\sigma_{k_z} = (m/\hbar)\sqrt{k_B T/m}$. Without loss of generality, one can assume that the z axis for this integration is chosen along $\boldsymbol{v}_{rec}$. Using

$$\int d^3 k_j \int d^3 k_l p(\boldsymbol{k}_j) p(\boldsymbol{k}_l) \exp\left(i v_{rec} t(k_{jz} - k_{lz})\right) = \exp\left(-(\sigma_{kz} v_{rec} t)^2\right), \tag{A.12}$$

one obtains

$$\langle \eta_{wr} \rangle_{avg} = \eta_0 \left(\frac{1}{N} + \frac{N^2 - N}{N^2} \exp\left(-(\sigma_{kz} v_{rec} t)^2\right)\right). \tag{A.13}$$

For $N > 1$, this results in a time- and temperature-dependent storage efficiency

$$\langle \eta_{wr} \rangle_{avg} = \eta_0 \left(\frac{1}{N} + \frac{N^2 - N}{N^2} \exp(-t^2/\tau^2)\right) \quad \text{with a } 1/e \text{ time} \quad \tau = \frac{\lambda_{dB}}{v_{rec}\sqrt{2\pi}}, \tag{A.14}$$

where $\lambda_{dB} = \hbar\sqrt{2\pi/m k_B T}$ is the thermal de Broglie wavelength. In Fig. A.1, the time-dependence is exemplified for several different temperatures.

For an atom number on the order of 10 to 15 atoms, one expects a decay on a time scale governed by the temperature. Due to the $1/N$ term in Eq. (A.13), the efficiency will not go down all the way to zero but will settle at a constant level determined both by the exact number of atoms and the finite efficiency at $t = 0$.

Bibliography

[1] E. Schrödinger. Discussion of Probability Relations between Separated Systems. *Mathematical Proceedings of the Cambridge Philosophical Society* **31**, 555–563 (1935).

[2] A. Einstein and M. Born. Brief vom 3. März 1947. In: *Briefwechsel 1916–1955*. Nymphenburger Verlagshandlung, München, (1991).

[3] A. Einstein, B. Podolski and N. Rosen. Can Quantum-Mechanical Description of Physical Reality Be Considered Complete? *Physical Review* **47**, 777–780 (1935).

[4] J. S. Bell. On the Einstein-Podolsky-Rosen paradox. *Physics* **1**, 195–200 (1964).

[5] J. S. Bell. On the Problem of Hidden Variables in Quantum Mechanics. *Reviews of Modern Physics* **38**, 447–452 (1966).

[6] J. F. Clauser, M. A. Horne, A. Shimony and R. A. Holt. Proposed Experiment to Test Local Hidden-Variable Theories. *Physical Review Letters* **23**, 880–884 (1969).

[7] J. F. Clauser and M. A. Horne. Experimental consequences of objective local theories. *Physical Review D* **10**, 526–535 (1974).

[8] S. J. Freedman and J. F. Clauser. Experimental Test of Local Hidden-Variable Theories. *Physical Review Letters* **28**, 938–941 (1972).

[9] A. Aspect, P. Grangier and G. Roger. Experimental Tests of Realistic Local Theories via Bell's Theorem. *Physical Review Letters* **47**, 460–463 (1981).

[10] A. Aspect, P. Grangier and G. Roger. Experimental Realization of Einstein-Podolsky-Rosen-Bohm *Gedankenexperiment* : A New Violation of Bell's Inequalities. *Physical Review Letters* **49**, 91–94 (1982).

[11] A. Aspect, J. Dalibard and G. Roger. Experimental Test of Bell's Inequalities Using Time-Varying Analyzers. *Physical Review Letters* **49**, 1804–1807 (1982).

[12] Z. Y. Ou and L. Mandel. Violation of Bell's Inequality and Classical Probability in a Two-Photon Correlation Experiment. *Physical Review Letters* **61**, 50–53 (1988).

[13] G. Weihs, T. Jennewein, C. Simon, H. Weinfurter and A. Zeilinger. Violation of Bell's Inequality under Strict Einstein Locality Conditions. *Physical Review Letters* **81**, 5039–5043 (1998).

[14] B. Weber, H. P. Specht, T. Müller, J. Bochmann, M. Mücke, D. L. Moehring and G. Rempe. Photon-Photon Entanglement with a Single Trapped Atom. *Physical Review Letters* **102**, 030501 (2009).

[15] M. Giustina, A. Mech, S. Ramelow, B. Wittmann, J. Kofler, J. Beyer, A. Lita, B. Calkins, T. Gerrits, S. W. Nam, R. Ursin and A. Zeilinger. Bell violation us-

ing entangled photons without the fair-sampling assumption. *Nature* **497**, 227–230 (2013).

[16] M. Lamehi-Rachti and W. Mittig. Quantum mechanics and hidden variables: A test of Bell's inequality by the measurement of the spin correlation in low-energy proton-proton scattering. *Physical Review D* **14**, 2543–2555 (1976).

[17] A. Bramon and M. Nowakowski. Bell Inequalities for Entangled Pairs of Neutral Kaons. *Physical Review Letters* **83**, 1–5 (1999).

[18] M. A. Rowe, D. Kielpinski, V. Meyer, C. A. Sackett, W. M. Itano, C. Monroe and D. J. Wineland. Experimental violation of a Bell's inequality with efficient detection. *Nature* **409**, 791–794 (2001).

[19] C. F. Roos, G. P. T. Lancaster, M. Riebe, H. Häffner, W. Hänsel, S. Gulde, C. Becher, J. Eschner, F. Schmidt-Kaler and R. Blatt. Bell States of Atoms with Ultralong Lifetimes and Their Tomographic State Analysis. *Physical Review Letters* **92**, 220402 (2004).

[20] Y. Hasegawa, R. Loidl, G. Badurek, M. Baron and H. Rauch. Violation of a Bell-like inequality in single-neutron interferometry. *Nature* **425**, 45–48 (2004).

[21] D. L. Moehring, M. J. Madsen, B. B. Blinov and C. Monroe. Experimental Bell Inequality Violation with an Atom and a Photon. *Physical Review Letters* **93**, 090410 (2004).

[22] D. N. Matsukevich, T. Chanelière, M. Bhattacharya, S.-Y. Lan, S. D. Jenkins, T. A. B. Kennedy and A. Kuzmich. Entanglement of a Photon and a Collective Atomic Excitation. *Physical Review Letters* **95**, 040405 (2005).

[23] J. Volz, M. Weber, D. Schlenk, W. Rosenfeld, J. Vrana, K. Saucke, C. Kurtsiefer and H. Weinfurter. Observation of Entanglement of a Single Photon with a Trapped Atom. *Physical Review Letters* **96**, 030404 (2006).

[24] J. Hofmann, M. Krug, N. Ortegel, L. Gerard, M. Weber, W. Rosenfeld and H. Weinfurter. Heralded Entanglement Between Widely Separated Atoms. *Science* **337**, 72–75 (2012).

[25] D. Salart, A. Baas, J. A. W. van Houwelingen, N. Gisin and H. Zbinden. Spacelike Separation in a Bell Test Assuming Gravitationally Induced Collapses. *Physical Review Letters* **100**, 220404 (2008).

[26] W. Rosenfeld, M. Weber, J. Volz, F. Henkel, M. Krug, A. Cabello, M. Zukowski and H. Weinfurter. Towards a Loophole-Free Test of Bell's Inequality with Entangled Pairs of Neutral Atoms. *Advanced Science Letters* 469–474 (2009).

[27] D. Kaiser. *How the Hippies Saved Physics: Science, Counterculture, and the Quantum Revival.* W.W. Norton & Company, New York (2011).

[28] P. Zoller, T. Beth, D. Binosi, R. Blatt, H. Briegel, D. Bruss, T. Calarco, J. I. Cirac, D. Deutsch, J. Eisert, A. Ekert, C. Fabre, N. Gisin, P. Grangiere, M. Grassl, S. Haroche, A. Imamoglu, A. Karlson, J. Kempe, L. Kouwenhoven, S. Kröll, G. Leuchs, M. Lewenstein, D. Loss, N. Lütkenhaus, S. Massar, J. E. Mooij, M. B. Plenio, E. Polzik, S. Popescu, G. Rempe, A. Sergienko, D. Suter, J. Twamley,

G. Wendin, R. Werner, A. Winter, J. Wrachtrup and A. Zeilinger. Quantum information processing and communication. *The European Physical Journal D* **36**, 203–228 (2005).

[29] E. Knill. Quantum computing. *Nature* **463**, 441–443 (2010).

[30] A. K. Ekert. Quantum cryptography based on Bell's theorem. *Physical Review Letters* **67**, 661–663 (1991).

[31] C. H. Bennett, G. Brassard, C. Crépeau, R. Jozsa, A. Peres and W. K. Wootters. Teleporting an unknown quantum state via dual classical and Einstein-Podolsky-Rosen channels. *Physical Review Letters* **70**, 1895–1899 (1993).

[32] K. Mattle, H. Weinfurter, P. G. Kwiat and A. Zeilinger. Dense Coding in Experimental Quantum Communication. *Physical Review Letters* **76**, 4656–4659 (1996).

[33] D. Deutsch. Quantum Theory, the Church-Turing Principle and the Universal Quantum Computer. *Proceedings of the Royal Society A: Mathematical, Physical and Engineering Sciences* **400**, 97–117 (1985).

[34] A. Ekert and R. Jozsa. Quantum algorithms: entanglement-enhanced information processing. *Philosophical Transactions of the Royal Society A: Mathematical, Physical and Engineering Sciences* **356**, 1769–1782 (1998).

[35] R. P. Feynman. Simulating physics with computers. *International Journal of Theoretical Physics* **21**, 467–488 (1982).

[36] S. Lloyd. Universal Quantum Simulators. *Science* **273**, 1073–1078 (1996).

[37] A. Trabesinger, J. Cirac, P. Zoller, I. Bloch, J. Dalibard, S. Nascimbéne, R. Blatt, C. Roos, A. Aspuru-Guzik, P. Walther, A. Houck, H. Türeci and J. Koch. Quantum Simulation. *Nature Physics Insight* **8**, 263–299 (2012).

[38] H.-K. Lo and H. F. Chau. Unconditional Security of Quantum Key Distribution over Arbitrarily Long Distances. *Science* **283**, 2050–2056 (1999).

[39] R. Ursin, F. Tiefenbacher, T. Schmitt-Manderbach, H. Weier, T. Scheidl, M. Lindenthal, B. Blauensteiner, T. Jennewein, J. Perdigues, P. Trojek, B. Ömer, M. Fürst, M. Meyenburg, J. Rarity, Z. Sodnik, C. Barbieri, H. Weinfurter and A. Zeilinger. Entanglement-based quantum communication over 144 km. *Nature Physics* **3**, 481–486 (2007).

[40] W. K. Wootters and W. H. Zurek. A single quantum cannot be cloned. *Nature* **299**, 802–803 (1982).

[41] D. Dieks. Communication by EPR devices. *Physics Letters A* **92**, 271–272 (1982).

[42] L. Lydersen, C. Wiechers, C. Wittmann, D. Elser, J. Skaar and V. Makarov. Hacking commercial quantum cryptography systems by tailored bright illumination. *Nature Photonics* **4**, 686–689 (2010).

[43] I. Gerhardt, Q. Liu, A. Lamas-Linares, J. Skaar, C. Kurtsiefer and V. Makarov. Full-field implementation of a perfect eavesdropper on a quantum cryptography system. *Nature Communications* **2**, 349 (2011).

[44] H. J. Briegel, W. Dür, J. I. Cirac and P. Zoller. Quantum Repeaters: The Role of

Imperfect Local Operations in Quantum Communication. *Physical Review Letters* **81**, 5932–5935 (1998).

[45] N. Sangouard, C. Simon, H. de Riedmatten and N. Gisin. Quantum repeaters based on atomic ensembles and linear optics. *Reviews of Modern Physics* **83**, 33–80 (2011).

[46] A. I. Lvovsky, B. C. Sanders and W. Tittel. Optical quantum memory. *Nature Photonics* **3**, 706–714 (2009).

[47] K. Hammerer, A. S. Sørensen and E. S. Polzik. Quantum interface between light and atomic ensembles. *Reviews of Modern Physics* **82**, 1041–1093 (2010).

[48] J. Wrachtrup and F. Jelezko. Processing quantum information in diamond. *Journal of Physics: Condensed Matter* **18**, S807–S824 (2006).

[49] H. de Riedmatten, M. Afzelius, M. U. Staudt, C. Simon and N. Gisin. A solid-state light-matter interface at the single-photon level. *Nature* **456**, 773–777 (2008).

[50] L.-M. Duan, M. D. Lukin, J. I. Cirac and P. Zoller. Long-distance quantum communication with atomic ensembles and linear optics. *Nature* **414**, 413–418 (2001).

[51] L.-M. Duan and C. Monroe. Quantum networks with trapped ions. *Reviews of Modern Physics* **82**, 1209–1224 (2010).

[52] A. Kuhn, M. Hennrich, T. Bondo and G. Rempe. Controlled generation of single photons from a strongly coupled atom-cavity system. *Applied Physics B: Lasers and Optics* **69**, 373–377 (1999).

[53] A. Kuhn, M. Hennrich and G. Rempe. Deterministic Single-Photon Source for Distributed Quantum Networking. *Physical Review Letters* **89**, (2002).

[54] J. McKeever, A. Boca, A. D. Boozer, R. Miller, J. R. Buck, A. Kuzmich and H. J. Kimble. Deterministic Generation of Single Photons from One Atom Trapped in a Cavity. *Science* **303**, 1992–1994 (2004).

[55] N. Akopian, N. Lindner, E. Poem, Y. Berlatzky, J. Avron, D. Gershoni, B. Gerardot and P. Petroff. Entangled Photon Pairs from Semiconductor Quantum Dots. *Physical Review Letters* **96**, 130501 (2006).

[56] P. C. Maurer, G. Kucsko, C. Latta, L. Jiang, N. Y. Yao, S. D. Bennett, F. Pastawski, D. Hunger, N. Chisholm, M. Markham, D. J. Twitchen, J. I. Cirac and M. D. Lukin. Room-Temperature Quantum Bit Memory Exceeding One Second. *Science* **336**, 1283–1286 (2012).

[57] M. Steger, K. Saeedi, M. L. W. Thewalt, J. J. L. Morton, H. Riemann, N. V. Abrosimov, P. Becker and H.-J. Pohl. Quantum information storage for over $180\,\mathrm{s}$ using donor spins in a ^{28}Si "semiconductor vacuum". *Science* **336**, 1280–1283 (2012).

[58] K. Saeedi, S. Simmons, J. Z. Salvail, P. Dluhy, H. Riemann, N. V. Abrosimov, P. Becker, H.-J. Pohl, J. J. L. Morton and M. L. W. Thewalt. Room-Temperature Quantum Bit Storage Exceeding 39 Minutes Using Ionized Donors in Silicon-28. *Science* **342**, 830–833 (2013).

[59] B. Lounis and M. Orrit. Single-photon sources. *Reports on Progress in Physics* **68**, 1129–1179 (2005).

[60] D. Jaksch, J. I. Cirac, P. Zoller, S. L. Rolston, R. Côté and M. D. Lukin. Fast Quantum Gates for Neutral Atoms. *Physical Review Letters* **85**, 2208–2211 (2000).

[61] L. Isenhower, E. Urban, X. L. Zhang, A. T. Gill, T. Henage, T. A. Johnson, T. G. Walker and M. Saffman. Demonstration of a Neutral Atom Controlled-NOT Quantum Gate. *Physical Review Letters* **104**, 010503 (2010).

[62] N. Timoney, I. Baumgart, M. Johanning, A. F. Varon, M. B. Plenio, A. Retzker and C. Wunderlich. Quantum gates and memory using microwave-dressed states. *Nature* **476**, 185–188 (2011).

[63] J. P. Home, D. Hanneke, J. D. Jost, J. M. Amini, D. Leibfried and D. J. Wineland. Complete methods set for scalable ion trap quantum information processing. *Science* **325**, 1227–1230 (2009).

[64] T. D. Ladd, F. Jelezko, R. Laflamme, Y. Nakamura, C. Monroe and J. L. O'Brien. Quantum computers. *Nature* **464**, 45–53 (2010).

[65] J. I. Cirac, P. Zoller, H. J. Kimble and H. Mabuchi. Quantum State Transfer and Entanglement Distribution among Distant Nodes in a Quantum Network. *Physical Review Letters* **78**, 3221–3224 (1997).

[66] J.-W. Pan, D. Bouwmeester, H. Weinfurter and A. Zeilinger. Experimental Entanglement Swapping: Entangling Photons That Never Interacted. *Physical Review Letters* **80**, 3891–3894 (1998).

[67] D. L. Moehring, P. Maunz, S. Olmschenk, K. C. Younge, D. N. Matsukevich, L.-M. Duan and C. Monroe. Entanglement of single-atom quantum bits at a distance. *Nature* **449**, 68–71 (2007).

[68] E. T. Jaynes and F. W. Cummings. Comparison of Quantum and Semiclassical Radiation Theories with Application to the Beam Maser. *Proc. IEEE* **51**, 889–109 (1963).

[69] K. Bergmann, H. Theuer and B. W. Shore. Coherent population transfer among quantum states of atoms and molecules. *Reviews of Modern Physics* **70**, 1003–1025 (1998).

[70] H. P. Specht, C. Nölleke, A. Reiserer, M. Uphoff, E. Figueroa, S. Ritter and G. Rempe. A single-atom quantum memory. *Nature* **473**, 190–193 (2011).

[71] M. Hennrich. Kontrollierte Erzeugung einzelner Photonen in einem optischen Resonator hoher Finesse. Doctoral thesis, Max-Planck-Institut für Quantenoptik & Technische Universität München (2003).

[72] A. Peres. Separability Criterion for Density Matrices. *Physical Review Letters* **77**, 1413–1415 (1996).

[73] M. Horodecki, P. Horodecki and R. Horodecki. Separability of mixed states: necessary and sufficient conditions. *Physics Letters A* **223**, 1–8 (1996).

[74] M. B. Plenio and S. Virmani. An introduction to entanglement measures. *Quantum Information and Computation* **7**, 1–51 (2007).

[75] S. J. van Enk, N. Lütkenhaus and H. J. Kimble. Experimental procedures for entanglement verification. *Physical Review A* **75**, 052318 (2007).

[76] G. Vidal and R. Werner. Computable measure of entanglement. *Physical Review A* **65**, 032314 (2002).

[77] J. B. Altepeter, E. R. Jeffrey and P. G. Kwiat. Photonic State Tomography. *Advances In Atomic, Molecular, and Optical Physics* **52**, 105–159 (2005).

[78] C. Nölleke. Quantum state transfer between remote single atoms. Doctoral thesis, Max-Planck-Institut für Quantenoptik & Technische Universität München (2013).

[79] T. Wilk. Quantum Interface between an Atom and a Photon. Ph.d. thesis, Max-Planck-Institut für Quantenoptik & Technische Universität München (2008).

[80] B. Weber. Distribution of Quantum Information between an Atom and Two Photons. Doctoral thesis, Max-Planck-Institut für Quantenoptik & Technische Universität München (2008).

[81] B. Terhal. Bell inequalities and the separability criterion. *Physics Letters A* **271**, 319–326 (2000).

[82] O. Gühne, P. Hyllus, D. Bruss, A. Ekert, M. Lewenstein, C. Macchiavello and A. Sanpera. Detection of entanglement with few local measurements. *Physical Review A* **66**, 062305 (2002).

[83] M. Mücke. Elektromagnetisch induzierte Transparenz mit einem einzelnen Atom. Doctoral thesis, Max-Planck-Institut für Quantenoptik & Technische Universität München (2011).

[84] M. Lettner. Ein Bose-Einstein-Kondensat als Quantenspeicher für Zwei-Teilchen-Verschränkung. Doctoral thesis, Max-Planck-Institut für Quantenoptik & Technische Universität München (2011).

[85] J. Bochmann. Coherent dynamics and state detection of single atoms in a cavity. Doctoral thesis, Max-Planck-Institut für Quantenoptik & Technische Universität München (2010).

[86] M. Hijlkema. Single photons from a single atom trapped in a high-finesse optical cavity. Doctoral thesis, Max-Planck-Institut für Quantenoptik & Technische Universität München (2007).

[87] S. Nußmann. Kühlen und Positionieren eines Atoms in einem optischen Resonator. Doctoral thesis, Max-Planck-Institut für Quantenoptik & Technische Universität München (2006).

[88] M. Hijlkema, B. Weber, H. P. Specht, S. C. Webster, A. Kuhn and G. Rempe. A single-photon server with just one atom. *Nature Physics* **3**, 253–255 (2007).

[89] M. Mücke, J. Bochmann, C. Hahn, A. Neuzner, C. Nölleke, A. Reiserer, G. Rempe and S. Ritter. Generation of single photons from an atom-cavity system. *Physical Review A* **87**, 063805 (2013).

[90] M. Keller, B. Lange, K. Hayasaka, W. Lange and H. Walther. Continuous generation of single photons with controlled waveform in an ion-trap cavity system. *Nature* **431**, 1075–1078 (2004).

[91] P. B. R. Nisbet-Jones, J. Dilley, D. Ljunggren and A. Kuhn. Highly efficient source for indistinguishable single photons of controlled shape. *New Journal of Physics* **13**,

103036 (2011).

[92] T. Legero, T. Wilk, M. Hennrich, G. Rempe and A. Kuhn. Quantum Beat of Two Single Photons. *Physical Review Letters* **93**, 070503 (2004).

[93] T. Wilk, S. C. Webster, H. P. Specht, G. Rempe and A. Kuhn. Polarization-Controlled Single Photons. *Physical Review Letters* **98**, 063601 (2007).

[94] T. Wilk, H. P. Specht, S. C. Webster, G. Rempe and A. Kuhn. Scheme for generating a sequence of single photons of alternating polarization. *Journal of Modern Optics* **54**, 1569–1580 (2007).

[95] S. Ritter, C. Nölleke, C. Hahn, A. Reiserer, A. Neuzner, M. Uphoff, M. Mücke, E. Figueroa, J. Bochmann and G. Rempe. An elementary quantum network of single atoms in optical cavities. *Nature* **484**, 195–200 (2012).

[96] T. Wilk, S. C. Webster, A. Kuhn and G. Rempe. Single-atom single-photon quantum interface. *Science* **317**, 488–490 (2007).

[97] T. Legero. Zeitaufgelöste Zwei-Photonen-Interferenz. Doctoral thesis, Max-Planck-Institut für Quantenoptik & Technische Universität München (2005).

[98] D. A. Steck. Rubidium 87 D Line Data. http://steck.us/alkalidata/ (Version 2.1.4) (2010).

[99] M. Lettner, M. Mücke, S. Riedl, C. Vo, C. Hahn, S. Baur, J. Bochmann, S. Ritter, S. Dürr and G. Rempe. Remote Entanglement between a Single Atom and a Bose-Einstein Condensate. *Physical Review Letters* **106**, 210503 (2011).

[100] C. Nölleke, A. Neuzner, A. Reiserer, C. Hahn, G. Rempe and S. Ritter. Efficient Teleportation Between Remote Single-Atom Quantum Memories. *Physical Review Letters* **110**, 140403 (2013).

[101] H. Specht. Einzelatom-Quantenspeicher für Polarisations-Qubits. Doctoral thesis, Max-Planck-Institut für Quantenoptik & Technische Universität München (2010).

[102] S. Massar and S. Popescu. Optimal Extraction of Information from Finite Quantum Ensembles. *Physical Review Letters* **74**, 1259–1263 (1995).

[103] A. V. Gorshkov, A. André, M. D. Lukin and A. S. Sørensen. Photon storage in Λ-type optically dense atomic media. I. Cavity model. *Phys. Rev. A* **76**, 033804 (2007).

[104] M. Mücke, E. Figueroa, J. Bochmann, C. Hahn, K. Murr, S. Ritter, C. J. Villas-Boas and G. Rempe. Electromagnetically induced transparency with single atoms in a cavity. *Nature* **465**, 755–8 (2010).

[105] U. Schnorrberger, J. D. Thompson, S. Trotzky, R. Pugatch, N. Davidson, S. Kuhr and I. Bloch. Electromagnetically Induced Transparency and Light Storage in an Atomic Mott Insulator. *Physical Review Letters* **103**, 033003 (2009).

[106] A. Reiserer, C. Nölleke, S. Ritter and G. Rempe. Ground-State Cooling of a Single Atom at the Center of an Optical Cavity. *Physical Review Letters* **110**, 223003 (2013).

[107] V. Winkler and A. Neuzner. Qubits und verschränkte Atome. *c't* **12**, 42–43 (2012).

[108] A. Reiserer, S. Ritter and G. Rempe. Nondestructive Detection of an Optical Photon. *Science* **342**, 1349–1351 (2013).

[109] C. W. Chou, H. de Riedmatten, D. Felinto, S. V. Polyakov, S. J. van Enk and H. J. Kimble. Measurement-induced entanglement for excitation stored in remote atomic ensembles. *Nature* **438**, 828–832 (2005).

[110] M. D. Eisaman, A. Andre, F. Massou, M. Fleischhauer, A. S. Zibrov and M. D. Lukin. Electromagnetically induced transparency with tunable single-photon pulses. *Nature* **438**, 837–841 (2005).

[111] S. Riedl, M. Lettner, C. Vo, S. Baur, G. Rempe and S. Dürr. Bose-Einstein condensate as a quantum memory for a photonic polarization qubit. *Physical Review A* **85**, 022318 (2012).

[112] D. Hunger, T. Steinmetz, Y. Colombe, C. Deutsch, T. W. Hänsch and J. Reichel. A fiber Fabry-Perot cavity with high finesse. *New Journal of Physics* **12**, 065038 (2010).

[113] M. Steiner, H. M. Meyer, C. Deutsch, J. Reichel and M. Köhl. Single Ion Coupled to an Optical Fiber Cavity. *Physical Review Letters* **110**, 043003 (2013).

[114] M. Fleischhauer, S. Yelin and M. Lukin. How to trap photons? Storing single-photon quantum states in collective atomic excitations. *Optics Communications* **179**, 395–410 (2000).

[115] J. Bochmann, M. Mücke, C. Guhl, S. Ritter, G. Rempe and D. L. Moehring. Lossless State Detection of Single Neutral Atoms. *Physical Review Letters* **104**, 203601 (2010).

[116] R. Gehr, J. Volz, G. Dubois, T. Steinmetz, Y. Colombe, B. L. Lev, R. Long, J. Estève and J. Reichel. Cavity-Based Single Atom Preparation and High-Fidelity Hyperfine State Readout. *Physical Review Letters* **104**, 203602 (2010).

[117] J. Volz, R. Gehr, G. Dubois, J. Esteve and J. Reichel. Measurement of the internal state of a single atom without energy exchange. *Nature* **475**, 210–213 (2011).

[118] R. B. Patel, A. J. Bennett, I. Farrer, C. A. Nicoll, D. A. Ritchie and A. J. Shields. Two-photon interference of the emission from electrically tunable remote quantum dots. *Nature Photonics* **4**, 632–635 (2010).

[119] R. Lettow, Y. L. a. Rezus, A. Renn, G. Zumofen, E. Ikonen, S. Götzinger and V. Sandoghdar. Quantum Interference of Tunably Indistinguishable Photons from Remote Organic Molecules. *Physical Review Letters* **104**, 123605 (2010).

[120] H. Bernien, L. Childress, L. Robledo, M. Markham, D. Twitchen and R. Hanson. Two-Photon Quantum Interference from Separate Nitrogen Vacancy Centers in Diamond. *Physical Review Letters* **108**, 043604 (2012).

[121] A. Sipahigil, M. Goldman, E. Togan, Y. Chu, M. Markham, D. Twitchen, A. Zibrov, A. Kubanek and M. Lukin. Quantum Interference of Single Photons from Remote Nitrogen-Vacancy Centers in Diamond. *Physical Review Letters* **108**, 143601 (2012).

[122] S. Nußmann, M. Hijlkema, B. Weber, F. Rohde, G. Rempe and A. Kuhn. Submicron Positioning of Single Atoms in a Microcavity. *Physical Review Letters* **95**, 173602

(2005).

[123] C. Langer, R. Ozeri, J. D. Jost, J. Chiaverini, B. DeMarco, A. B. Kish, R. B. Blakestad, J. Britton, D. B. Hume, W. M. Itano, D. Leibfried, R. Reichle, T. Rosenband, T. Schaetz, P. O. Schmidt and D. J. Wineland. *Long-Lived Qubit Memory Using Atomic Ions. Physical Review Letters* **95**, 060502 (2005).

Publications

Generation of single photons from an atom-cavity system
M. Mücke, J. Bochmann, C. Hahn, A. Neuzner, C. Nölleke, A. Reiserer, G. Rempe, and
S. Ritter
Physical Review A **87**, 063805 (2013)

Efficient Teleportation between remote Single Atom Quantum Memories
C. Nölleke, A. Neuzner, A. Reiserer, C. Hahn, G. Rempe, and S. Ritter
Physical Review Letters **110**, 140403 (2013)

An elementary quantum network of single atoms in optical cavities
S. Ritter, C. Nölleke, C. Hahn, A. Reiserer, A. Neuzner, M. Uphoff, M. Mücke, E. Figueroa,
J. Bochmann, and G. Rempe
Nature **484**, 195 (2012)

Remote Entanglement between a Single Atom and a Bose-Einstein-Condensate
M. Lettner, M. Mücke, S. Riedl, C. Vo, C. Hahn, S. Baur, J. Bochmann, S. Ritter, S.
Dürr, and G. Rempe
Physical Review Letters **106**, 210503 (2011)

Electromagnetically induced transparency with single atoms in a cavity
M. Mücke, E. Figueroa, J. Bochmann, C. Hahn, K. Murr, S. Ritter, C. J. Villas-Boas, and
G. Rempe
Nature **465**, 755 (2010).

Dankeschön!

Zum Gelingen dieser Arbeit haben in den letzten Jahren viele Menschen auf die unterschiedlichste Art und Weise beigetragen. Ihnen möchte ich an dieser Stelle ein herzliches Dankeschön aussprechen!

Mein erster Dank gilt dabei meinem Doktorvater Prof. Dr. Gerhard Rempe für das entgegengebrachte Vertrauen und die Chance, an so spannenden und faszinieren Experimenten mitwirken zu dürfen.

Im Großteil meiner Laborzeit ging es um quantenphysikalisches Netzwerkeln – erst um das Verschränken eines Einzalatoms mit einem Bose-Einstein Kondensat und später um Kopplungsexperimente mit zwei einzelnen Atomen. Meinen Kollegen danke ich für die große Professionalität und die freundschaftliche Zusammenarbeit bei diesen anspruchsvollen und bisweilen durchaus nervenzehrenden Messungen.

In unserem Labor, dem 'Netzwerkknoten A', habe ich im ersten Jahr von Martin Mücke gelernt, was es bedeutet, so ein komplexes Experiment zu zähmen. Nicht zuletzt die wertvollen Erfahrungen aus unserer Verschränkung mit dem BEC-Experiment sind unserem zweiten Kopplungsabenteuer zugute gekommen, für das Jörg Bochmann als Postdoc an seine alte Apparatur zurückgekehrt ist. Die gemeinsame Zeit mit ihm im und auch außerhalb des Labors war mir eine große Freude. Andi Neuzner hat mit beeindruckender technischer Finesse und seiner enormen Begeisterungsfähigkeit das Experiment weit über die Netzwerkphase hinaus sehr bereichert. Als unser einziger 'Masterand' hat André Kochanke mit seiner fröhlichen Art die Arbeitsatmosphäre beflügelt.

Ein großes Dankeschön geht natürlich auch ans andere Ende der Quantenleitung, an den 'Netzwerkknoten B', wo Christian Nölleke und Andi Reiserer ausgezeichnete Arbeit geleistet haben, unterstützt von Manuel Uphoff und Eden Figueroa, sowie, in den Zeiten vor und nach den gemeinsamen Messungen, von Holger Specht und Norbert Kalb. Ohne Euch hätte es die erste Quanten-LAN-Party noch nicht gegeben!

Stephan Ritter hat als Postdoc die losen Enden des Netzwerks verbunden, und ich danke ihm für die zuverlässige Hilfestellung im Labor, für seinen wertvollen fachlichen Rat und seine Unterstützung beim Lösen der verrücktesten Probleme. Dave Moehring danke ich für die entscheidende Motivation, an diesem und keinem anderen Experiment zu promovieren.

Unseren Koppel-Kumpanen vom benachbarten BEC-Labor, Matthias Lettner, Chris Vo, Stephan Riedl und Simon Baur, danke ich für die gemeinsame Zeit und die guten Nachbarschaft. Stephan Dürr war als wandelndes Lexikon ein ausgezeichneter Ansprechpartner für jegliche Physikfragen. Ihm danke ich insbesondere für den entscheidenen Beitrag zum Verständnis dessen, was schiefgehen kann, wenn man zur Abwechslung nicht mit einem sondern mit vielen Atomen arbeitet, siehe Anhang A.

Die tatkräftige Unterstützung unserer Techniker Sepp Bayerl, Franz Denk, Helmuth Stehbeck, Tobi Urban und Tom Wiesmeier war ähnlich unentbehrlich wie die unserer anderen